© 2015. Published by The Company of Biologists Ltd | Development (2015) 142, 2860 doi:10.1242/dev.128751

CORRECTION

Intraflagellar transport 27 is essential for hedgehog signaling but dispensable for ciliogenesis during hair follicle morphogenesis

Ning Yang, Li Li, Thibaut Eguether, John P. Sundberg, Gregory J. Pazour and Jiang Chen

There was an error published in *Development* **142**, 2194-2202.

On p. 2200, Ng et al. (2012) was incorrectly cited in place of Liew et al. (2014). The corrected text and reference appear below. The authors apologise to readers for this mistake.

IFT27 was recently shown to play a crucial role in facilitating ciliary exit of the BBSome (Eguether et al., 2014; Liew et al., 2014), and *Ift27*-deficient mouse embryonic fibroblasts are unable to maintain low levels of SMO in the cilia when the Hh pathway is inactive (Eguether et al., 2014).

Liew, G. M., Ye, F., Nager, A. R., Murphy, J. P., Lee, J. S., Aguiar, M., Breslow, D. K., Gygi, S. P. and Nachury, M. V. (2014). The intraflagellar transport protein IFT27 promotes BBSome exit from cilia through the GTPase ARL6/BBS3. *Dev. Cell* **31**, 265-278.

© 2015. Published by The Company of Biologists Ltd | Development (2015) 142, 2194-2202 doi:10.1242/dev.115261

RESEARCH ARTICLE

Intraflagellar transport 27 is essential for hedgehog signaling but dispensable for ciliogenesis during hair follicle morphogenesis

Ning Yang[1], Li Li[2], Thibaut Eguether[3], John P. Sundberg[4], Gregory J. Pazour[3] and Jiang Chen[1,*]

ABSTRACT

Hair follicle morphogenesis requires precisely controlled reciprocal communications, including hedgehog (Hh) signaling. Activation of the Hh signaling pathway relies on the primary cilium. Disrupting ciliogenesis results in hair follicle morphogenesis defects due to attenuated Hh signaling; however, the loss of cilia makes it impossible to determine whether hair follicle phenotypes in these cilia mutants are caused by the loss of cilia, disruption of Hh signaling, or a combination of these events. In this study, we characterized the function of *Ift27*, which encodes a subunit of intraflagellar transport (IFT) complex B. Hair follicle morphogenesis of *Ift27*-null mice was severely impaired, reminiscent of phenotypes observed in cilia and Hh mutants. Furthermore, the Hh signaling pathway was attenuated in *Ift27* mutants, which was in association with abnormal ciliary trafficking of SMO and GLI2, and impaired processing of Gli transcription factors; however, formation of the ciliary axoneme was unaffected. The ciliary localization of IFT25 (HSPB11), the binding partner of IFT27, was disrupted in *Ift27* mutant cells, and *Ift25*-null mice displayed hair follicle phenotypes similar to those of *Ift27* mutants. These data suggest that *Ift27* and *Ift25* operate in a genetically and functionally dependent manner during hair follicle morphogenesis. This study suggests that the molecular trafficking machineries underlying ciliogenesis and Hh signaling can be segregated, thereby providing important insights into new avenues of inhibiting Hh signaling, which might be adopted in the development of targeted therapies for Hh-dependent cancers, such as basal cell carcinoma.

KEY WORDS: Intraflagellar transport, *Ift27*, Hedgehog signaling, Cilia, Hair follicle, Skin, Mouse

INTRODUCTION

The development of the skin starts with the commitment of single-layered surface ectoderm to stratification controlled by the transcription factor TRP63 (Candi et al., 2008, 2007), followed by the terminal differentiation of epidermal keratinocytes (Blanpain et al., 2006). The induction of hair follicle formation is initiated by reciprocal interactions between epidermal keratinocytes and folliculogenic dermal papilla cells mediated by molecular signaling pathways, notably canonical Wnt signaling (Schmidt-Ullrich and Paus, 2005). Further development of the hair follicle is marked by downward growth and maturation as a result of follicular keratinocyte proliferation and differentiation (Schmidt-Ullrich and Paus, 2005), which requires hedgehog (Hh) signaling (Schmidt-Ullrich and Paus, 2005). Prior studies demonstrated that disrupting genes involved in Hh signaling could result in complete arrest of hair follicle development (Chiang et al., 1999; Mill et al., 2003; St-Jacques et al., 1998; Woo et al., 2012), revealing Hh signaling as an indispensable signaling mechanism during early stages of hair follicle morphogenesis.

In vertebrates, the primary cilium, which is an antenna-like cellular protrusion, serves as the venue for Hh signaling (Corbit et al., 2005; Huangfu and Anderson, 2005; Wong et al., 2009). When the Hh signaling pathway is inactive, Hh receptor PTCH1 occupies the ciliary membrane, suppressing SMO. Upon binding of ligand, such as sonic hedgehog (SHH), the suppression by PTCH1 is relieved, permitting SMO to be activated (Rohatgi et al., 2007; Wang et al., 2009a), thereby activating Gli transcription factors and the expression of downstream target genes (Haycraft et al., 2005; Kim et al., 2009; Tukachinsky et al., 2010). In addition, the primary cilium is essential for the proteolytic processing of Gli factors into transcriptional repressors in the absence of the ligand (Haycraft et al., 2005; Huangfu and Anderson, 2005). A number of recent studies demonstrated that disrupting cilia formation results in developmental arrest of hair follicles by suppressing Hh signaling (Chen et al., 2015; Dai et al., 2013, 2011; Lehman et al., 2009). These studies confirmed the integral role of primary cilia in mediating the epithelial-mesenchymal crosstalk required for hair follicle morphogenesis. However, the loss of the ciliary axoneme in these mutants made it impossible to understand whether the attenuated Hh signaling was caused by the loss of cilia, defective trafficking of Hh components, or a combination of both.

The assembly of the ciliary axoneme and the processing of Hh signals require intraflagellar transport (IFT) (Huangfu et al., 2003). IFT is an evolutionarily conserved intracellular trafficking mechanism, which was first characterized in *Chlamydomonas reinhardtii* (Kozminski et al., 1993). All IFT proteins identified in *Chlamydomonas* are found in mammals (Cole and Snell, 2009; Follit et al., 2009). The IFT system comprises IFT-A and IFT-B protein complexes. Both IFT-A and IFT-B are essential for cilia assembly and maintenance, as well as the transduction of molecular signals. IFT-B seems to be more fundamental for ciliary assembly, whereas IFT-A plays a role in retrograde transport and the entry of some G-protein-coupled receptors into cilia (Cole et al., 1998; Follit et al., 2009; Rosenbaum and Witman, 2002). Disrupting subunits of IFT complexes could result in the loss of the ciliary axoneme and attenuated Hh signaling (Houde et al., 2006; Huangfu et al., 2003).

IFT27 belongs to the IFT-B complex (Qin et al., 2007). In contrast to other IFT proteins, IFT27 does not have homologs in *Caenorhabditis elegans* or *Drosophila melanogaster*, which do not rely on primary cilia to process Hh signals, suggesting that IFT27 might possess unique roles in ciliogenesis and Hh signaling in comparison to other IFT proteins. IFT27 is a small Rab-like GTPase

[1]Departments of Pathology and Dermatology, Stony Brook University, Stony Brook, NY 11794, USA. [2]Department of Dermatology, Peking Union Medical College Hospital, Beijing 100730, China. [3]Program in Molecular Medicine, University of Massachusetts Medical School, Worcester, MA 01605, USA. [4]The Jackson Laboratory, Bar Harbor, ME 04609, USA.

*Author for correspondence (jiang.chen@stonybrook.edu)

Received 11 July 2014; Accepted 1 May 2015

Development (2015) 142, 2194-2202 doi:10.1242/dev.115261

that is capable of forming a heterodimer with IFT25 (HSPB11) (Bhogaraju et al., 2011; Cole, 2003; Wang et al., 2009b). In a previous study, we discovered that IFT25 is dispensable for cilia assembly but remains essential for the trafficking of Hh signaling molecules in cilia (Keady et al., 2012). It is particularly intriguing to know whether these intracellular trafficking molecules are essential for the transduction of molecular signals in the context of epithelial-mesenchymal interaction during the development of multicellular organs.

Here, we examined the role of *Ift27* during embryonic development of the skin and found that disrupting *Ift27* expression blocks hair follicle morphogenesis. The hair follicle phenotype was associated with attenuated Hh signaling in *Ift27* mutant skin. Accordingly, primary dermal fibroblasts isolated from *Ift27* mutants were unable to respond to Hh pathway activation. Interestingly, the formation of primary cilia was unaffected in *Ift27* mutant cells and we found that disrupted Hh signaling was associated with the abnormal ciliary accumulation of SMO in *Ift27* mutant cells. Moreover, the ciliary localization of IFT25 was disrupted in *Ift27* mutant cells, and *Ift25* mutant mice displayed hair follicle phenotypes similar to those of *Ift27* mutants. Thus, data obtained from this study suggest that *Ift27* and *Ift25* may operate in a molecularly and functionally interdependent fashion during hair follicle formation through regulating ciliary trafficking of Hh pathway components.

RESULTS

Expression of *Ift27* in the mouse skin and hair follicle

To understand the relevance of *Ift27* in skin development, we examined *Ift27* expression at the transcriptional and translational levels. *Ift27* mRNA and protein were expressed throughout embryonic skin development (supplementary material Fig. S1A; Fig. 1A,B). Interestingly, IFT27 levels decreased significantly in P28 skin ($P<0.05$), which is concomitant with the completion of hair follicle morphogenesis and the entrance into the first hair cycle. Furthermore, quantitative RT-PCR and *in situ* hybridization demonstrated that *Ift27* mRNA is expressed in both epidermis and dermis (supplementary material Fig. S1B; Fig. 1C,C′), including follicular keratinocytes and dermal papilla cells of developing hair follicles (Fig. 1C,C′).

By contrast, *Ift27* mRNA and protein were undetectable in hair follicles or skin of homozygous *Ift27* mutants (Fig. 1C″,D,E). Thus, the homozygous *Ift27* mutants are essentially *Ift27*-null mutants and are hereafter referred as $Ift27^{-/-}$. Throughout this study, phenotypes observed in heterozygous mice ($Ift27^{+/-}$) were indistinguishable from those of wild-type littermates (data not shown), and the wild-type littermates ($Ift27^{+/+}$) were used as controls.

Disrupting *Ift27* blocks the differentiation of follicular keratinocytes but not epidermal keratinocytes

The dorsal skin of mutant embryos was examined for developmental abnormalities. Hematoxylin and Eosin (H&E) staining of E14.5 and E15.5 skin did not reveal any apparent defects in $Ift27^{-/-}$ embryos (supplementary material Fig. S2A and Fig. S3A). Furthermore, immunofluorescence labeling of TRP63, KRT14, KRT1, LOR (Fig. 2B; supplementary material Fig. S2B,C and Fig. S3B), BrdU labeling (Fig. 2C; supplementary material Fig. S3G,H and Fig. S4A) and TUNEL assay (data not shown) revealed normal epidermal stratification, differentiation, proliferation and apoptosis in $Ift27^{-/-}$ skin throughout early (E14.5) and late (E18.5) stages of epidermal development. The expression levels of canonical Wnt and Notch target genes and the activation of BMP and TGFβ signaling pathways were also unchanged in $Ift27^{-/-}$ skin (supplementary material Fig. S4B-E). These observations suggest that *Ift27* is unlikely to be involved in embryonic development of the epidermis. However, the E18.5 $Ift27^{-/-}$ skin displayed a striking hair follicle phenotype, in which the majority of hair follicles were substantially reduced in size (Fig. 2A). Therefore, we focused our investigation on the formation of hair follicles.

Classification of the developmental stages of hair follicles based on morphological features described by Paus et al. (1999) revealed that the development of hair follicles in $Ift27^{-/-}$ skin was significantly delayed. Specifically, in E18.5 control skin, the percentage of stage 1-2, 3-4 and stage 5-6 hair follicles was 29.3±17.9%, 41.8±9.7% and 28.8±21.3%, respectively. In the $Ift27^{-/-}$ skin, up to 90.1% of hair follicles remained in stage 1-2 ($P<0.001$), whereas only 0.7% developed beyond stage 5 ($P<0.01$) (Fig. 2D). Interestingly, the number of hair follicles (irrespective of their differentiation stages) was only slightly reduced in $Ift27^{-/-}$ skin at E18.5 ($P=0.11$;

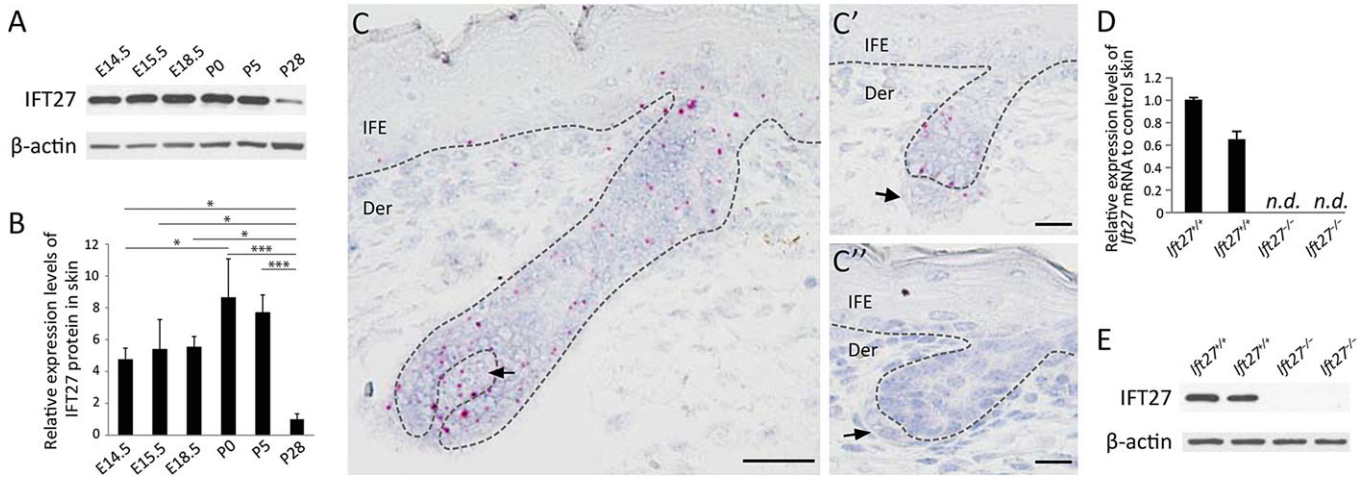

Fig. 1. *Ift27* is essential for hair follicle development. (A,B) Expression of IFT27 protein in mouse skin by western blotting (A) and quantification relative to P28 (set at 1) (B). $n=4$; *$P<0.05$, ***$P<0.001$. (C) *In situ* hybridization of *Ift27* transcripts in the dorsal skin of the E18.5 mouse embryo. (C′,C″) Representative stage 2 hair follicles in control (C′) and $Ift27^{-/-}$ (C″) skin. Dashed lines indicate the epidermal-dermal junction. Arrows point to dermal papilla cells. IFE, interfollicular epidermis; Der, dermis. (D,E) Expression of *Ift27* mRNA (D) and protein (E) in the skin of E18.5 control ($Ift27^{+/+}$) and $Ift27^{-/-}$. n.d., not detectable. Scale bars: 100 µm in C; 50 µm in C′,C″.

Development (2015) 142, 2194-2202 doi:10.1242/dev.115261

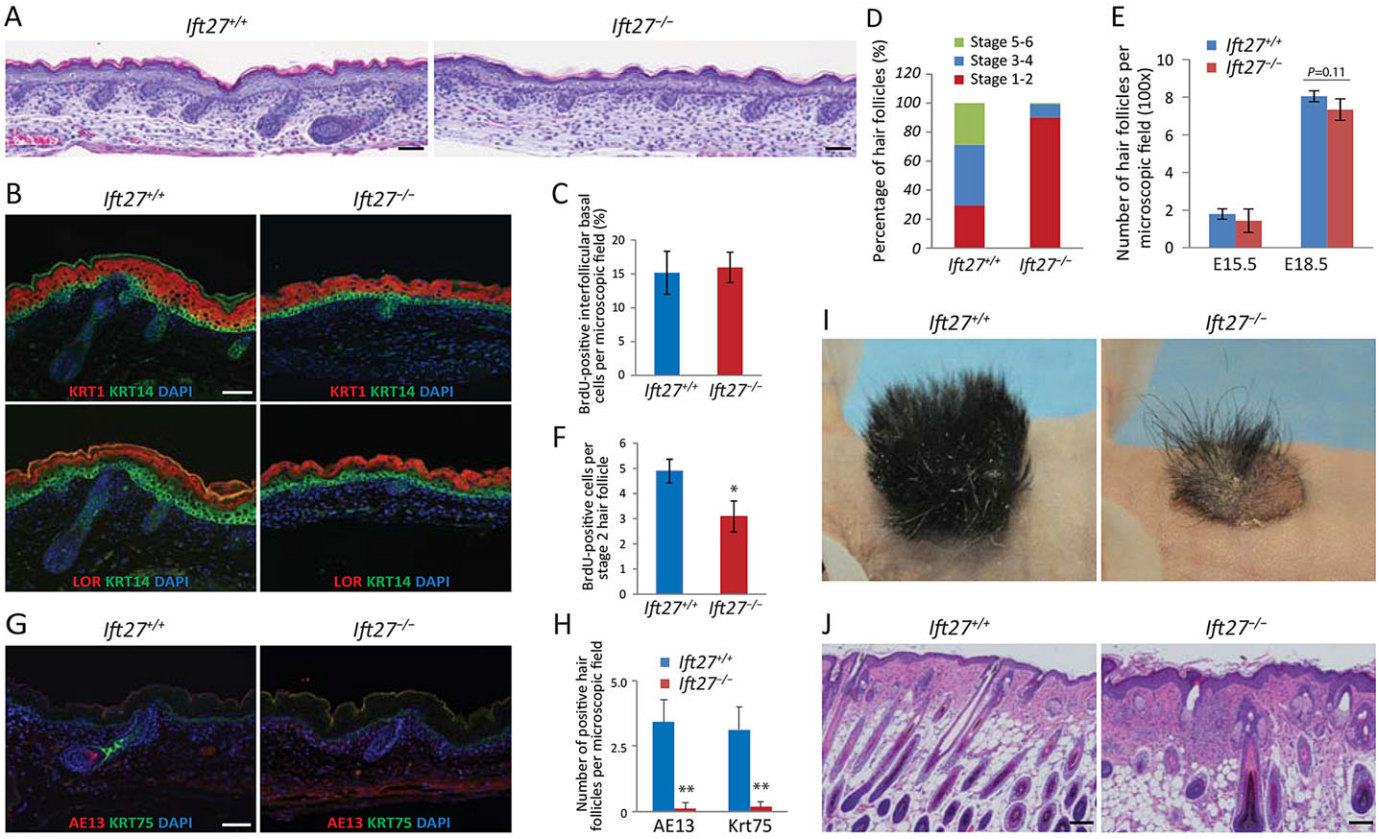

Fig. 2. Skin and hair follicle phenotypes of *Ift27*$^{-/-}$ embryos. (A) Representative histology (H&E staining) of E18.5 control (*Ift27*$^{+/+}$) and *Ift27*$^{-/-}$ dorsal skin. (B) Expression of differentiation markers of the epidermis at E18.5. There is no apparent difference in the expression profiles of KRT1 and LOR in control and *Ift27*$^{-/-}$. (C) BrdU^{+} cells in the basal layer of the interfollicular epidermis of E18.5 *Ift27*$^{+/+}$ and *Ift27*$^{-/-}$. (D) Distribution of the developmental stages of hair follicles of E18.5 dorsal skin. A minimum of 100 hair follicles were analyzed; $n \geq 6$. (E) Number of hair follicles in E15.5 and E18.5 control and *Ift27*$^{-/-}$ dorsal skin per microscopy field (100×); $n \geq 4$. (F) BrdU^{+} follicular keratinocytes in stage 2 hair follicles of E18.5 control and *Ift27*$^{-/-}$. (G,H) Representative images (G) and statistical analysis (H) of double immunofluorescence labeling of AE13 (red) and KRT75 (green) of hair follicles in E18.5 control and *Ift27*$^{-/-}$ skin. (I,J) Representative gross appearance (I) and histology (H&E staining, J) of skin transplants at 35 days post-transplantation. **P*<0.05, ***P*<0.01. Scale bars: 50 µm in A,B,G; 100 µm in J.

Fig. 2E), but the number of proliferating cells in *Ift27*$^{-/-}$ hair follicles was markedly reduced (*P*<0.01; Fig. 2F; supplementary material Fig. S4A). Thus, the data obtained so far suggested that delayed hair follicle development in *Ift27*$^{-/-}$ embryos was likely to be associated with impaired responses to mitogenic signals.

Examination of hair follicle differentiation markers, such as KRT75 (companion cell layer) and AE13 (hair cortex), demonstrated that 3.4±0.8 and 3.1±0.9 wild-type hair follicles (per microscopic field) expressed these markers, respectively (Fig. 2G,H), compared with only 0.1±0.2 and 0.2±0.2 hair follicles in *Ift27*$^{-/-}$ skin (*P*<0.001; Fig. 2G,H). This observation strongly suggests that delayed hair follicle development in *Ift27*$^{-/-}$ skin is caused by abnormal follicular keratinocyte differentiation.

By contrast, the induction of hair follicle formation was indistinguishable between *Ift27*$^{-/-}$ and control skin. Specifically, the number and expression pattern of KRT17^{+} hair germs in E15.5 *Ift27*$^{-/-}$ skin were comparable to those in wild-type littermates (supplementary material Fig. S3C). Moreover, the expression of LEF1 (supplementary material Fig. S3D), a marker for the activation of canonical Wnt signaling, and of NGFR (formerly known as p75NTR) (supplementary material Fig. S3E), alkaline phosphatase (AP) activity (supplementary material Fig. S3F) and the number of BrdU^{+} follicular keratinocytes (supplementary material Fig. S3G,H) were comparable in early stage control and *Ift27*$^{-/-}$ hair follicles.

Because *Ift27*$^{-/-}$ mice die shortly after birth we could not determine whether the development of hair follicles was temporarily delayed or impermissible in these animals. To address this question, dorsal skin of E18.5 *Ift27*$^{-/-}$ mutants was transplanted onto nude (*Foxn1*^{nu}) mice for further development and maturation. *Ift27*$^{-/-}$ skin was able to engraft. However, there was a drastic reduction in the number of hairs in the *Ift27*$^{-/-}$ skin (Fig. 2I). H&E staining of tissues collected 5 weeks post-grafting confirmed that the hair phenotype was due to the lack of hair follicles (Fig. 2J). Thus, disrupting *Ift27* blocked hair follicle development.

Hh signaling is perturbed in *Ift27*$^{-/-}$ skin

The hair follicle phenotype of *Ift27*$^{-/-}$ mice was reminiscent of that of Hh mutants (Chiang et al., 1999; Gat et al., 1998; Mill et al., 2003; St-Jacques et al., 1998; Woo et al., 2012). Consistently, *in situ* hybridization and quantitative RT-PCR revealed that *Ift27*$^{-/-}$ skin (E15.5 and E18.5) had significantly reduced expression levels of Hh target genes, such as *Gli1* and *Ptch1*, in follicular keratinocytes and dermal papilla cells (Fig. 3A-C; supplementary material Fig. S5A,B). Interestingly, the expression of *Shh* was essentially indistinguishable between control and *Ift27*$^{-/-}$ embryos (*P*=0.08; Fig. 3C; supplementary material Fig. S5C). Moreover, western blotting revealed reduced processing of full-length GLI3 (GLI3-FL) to GLI3 repressor (GLI3-R) in skin biopsied from E18.5 *Ift27* mutants (Fig. 3D), which led to an increased GLI3-FL:GLI3-R ratio (Fig. 3D). These findings suggest that perturbation of the Hh pathway is likely to have occurred downstream of ligand but upstream of Gli transcription factors.

Development (2015) 142, 2194-2202 doi:10.1242/dev.115261

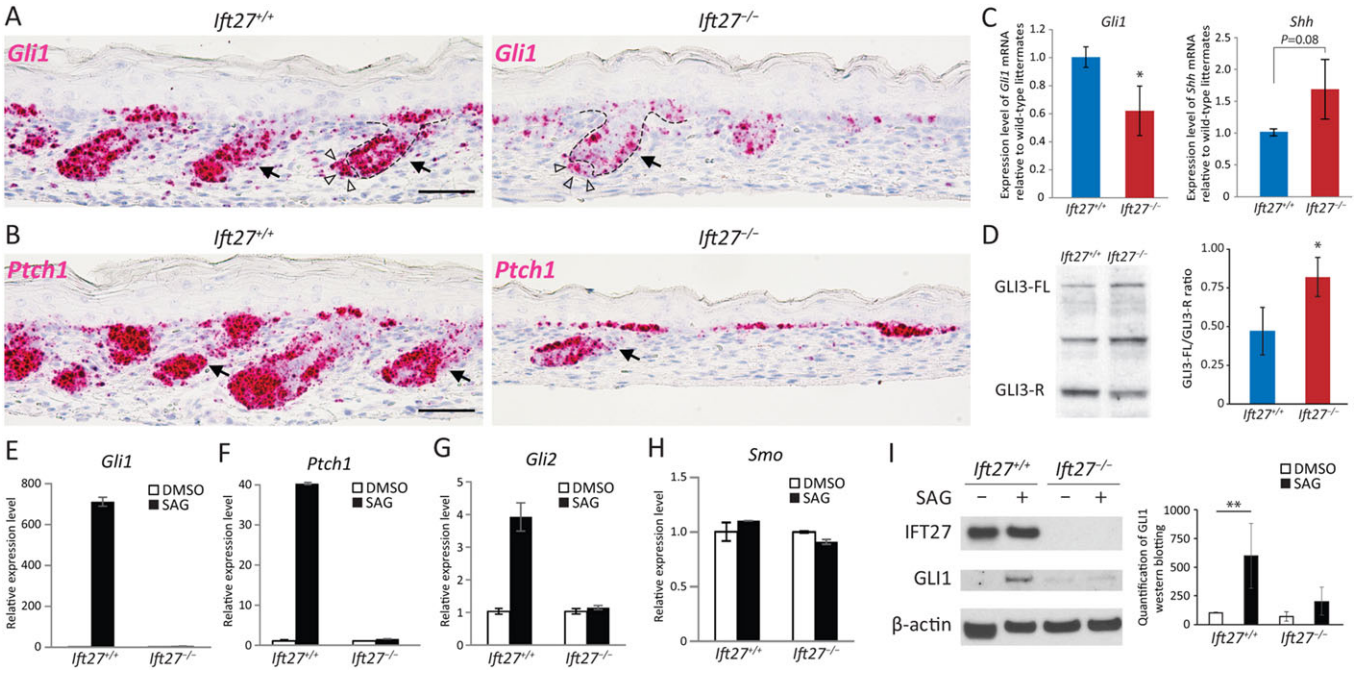

Fig. 3. Hh signaling is attenuated in *Ift27*$^{-/-}$ skin. (A,B) *In situ* hybridization of *Gli1* (A) and *Ptch1* (B) in E18.5 control (*Ift27*$^{+/+}$) and *Ift27*$^{-/-}$ skin; *n*=3. Arrows indicate hair follicles of similar stages; arrowheads point to dermal papilla cells; dashed line delineates the epidermal-dermal junction. (C) Relative expression levels of *Gli1* and *Shh* in the skin of E18.5 *Ift27*$^{+/+}$ and *Ift27*$^{-/-}$ embryos by quantitative RT-PCR; *n*=4. (D) Expression of full-length (GLI3-FL) and repressor (GLI3-R) forms of GLI3 in skin of E18.5 control and *Ift27* mutants. (E-H) Responses of *Ift27*$^{+/+}$ and *Ift27*$^{-/-}$ primary dermal fibroblasts to SAG treatment as determined by the relative expression levels of *Gli1* (E), *Ptch1* (F), *Gli2* (G) and *Smo* (H); *n*=3. (I) Representative western blotting of IFT27 and GLI1 in SAG-treated *Ift27*$^{+/+}$ and *Ift27*$^{-/-}$ dermal fibroblasts and quantification of GLI1; *n*=4. **P*<0.05, ***P*<0.01 (two-way ANOVA and Bonferroni post-test). Scale bars: 100 µm.

To further determine how *Ift27* participates in transducing Hh signals during hair follicle development, primary dermal fibroblasts were treated with SMO agonist (SAG) and the expression of Hh-responsive genes examined. SAG treatment drastically induced the expression of Hh target genes (*Ptch1*, *Gli1* and *Gli2*) in control cells, a response that was attenuated in *Ift27*$^{-/-}$ cells (Fig. 3E-G,I). By contrast, the expression of *Smo* was unaffected (Fig. 3H). IFT27 was essentially undetectable in *Ift27*$^{-/-}$ cells by western blotting (Fig. 3I). These data obtained from primary dermal fibroblasts were consistent with *in vivo* findings, thereby strengthening the idea that IFT27 participates in Hh signaling downstream of SMO activation. Moreover, primary dermal fibroblasts of *Ift27*$^{-/-}$ mice demonstrated increased GLI3-FL levels and an increased GLI3-FL:GLI3-R ratio (supplementary material Fig. S6), suggesting that the processing of Gli transcription factors was disrupted in *Ift27*$^{-/-}$ cells.

Formation of the ciliary axoneme is unaffected in *Ift27*$^{-/-}$ skin

Because Hh signaling requires primary cilia and the formation of cilia requires IFT, we speculated that *Ift27* might be essential for Hh signaling by controlling ciliogenesis in follicular keratinocytes and dermal papilla cells. Immunofluorescence labeling with a number of ciliary markers, namely ARL13B, ADCY3 (ACIII) and acetylated α-tubulin, revealed indistinguishable patterns of primary cilia in wild-type and *Ift27*$^{-/-}$ skin at various developmental stages (Fig. 4A; supplementary material Fig. S7; data not shown). Scanning electron microscopy of primary keratinocytes isolated from control and *Ift27*$^{-/-}$ embryos also revealed primary cilia of comparable appearance (supplementary material Fig. S8). Thus, these observations suggested that neither the formation of the ciliary axoneme nor the localization of ciliary membrane-associated proteins, such as ARL13B and ADCY3, was affected in *Ift27*$^{-/-}$ cells.

Skin transplants generated from control embryos contained an abundance of ciliated follicular keratinocytes (supplementary material Fig. S9A). Remarkably, cells in the epidermal invaginations of *Ift27*$^{-/-}$ skin transplants also contained well-ciliated keratinocytes (supplementary material Fig. S9B). These cells are proposed to be keratinocytes that are committed to the follicular fate but have failed to develop into hair follicles because of disrupted Hh signaling or primary cilia formation (Chen et al., 2015; Chiang et al., 1999; Dai et al., 2013, 2011; Gat et al., 1998; Mill et al., 2003; St-Jacques et al., 1998). Thus, the congregation of these ciliated keratinocytes in the epidermal invaginations of *Ift27*$^{-/-}$ skin transplants not only confirmed this speculation but also strengthened our previous observation that *Ift27* is essential for Hh signaling (Fig. 3) but not for primary cilia formation (Fig. 4).

To further examine the ciliogenic potential of *Ift27*$^{-/-}$ cells, primary keratinocytes were treated with cytochalasin D (cyto D), a compound capable of elongating the ciliary axoneme. Twenty-four hours after cyto D treatment (0.5 µM), the number of ciliated cells remained unchanged in both wild-type and *Ift27*$^{-/-}$ keratinocytes (Fig. 4C) and the median length of the ciliary axoneme increased significantly in both genotypes (*P*<0.0001; Fig. 4B,D).

Thus, data obtained from *in vivo* and *in vitro* experiments strongly suggest that *Ift27* does not participate in ciliogenesis or ciliary maintenance in epidermal keratinocytes.

Ciliary localization of SMO is disrupted in *Ift27*$^{-/-}$ primary dermal fibroblasts

To gain insight into how *Ift27* regulates the Hh pathway, we examined the ciliary localization of Hh pathway components in primary dermal fibroblasts isolated from E18.5 mouse embryos. Similar to what was observed in *Ift27*$^{-/-}$ keratinocytes, *Ift27*$^{-/-}$ primary dermal fibroblasts were capable of forming primary cilia

Development (2015) 142, 2194-2202 doi:10.1242/dev.115261

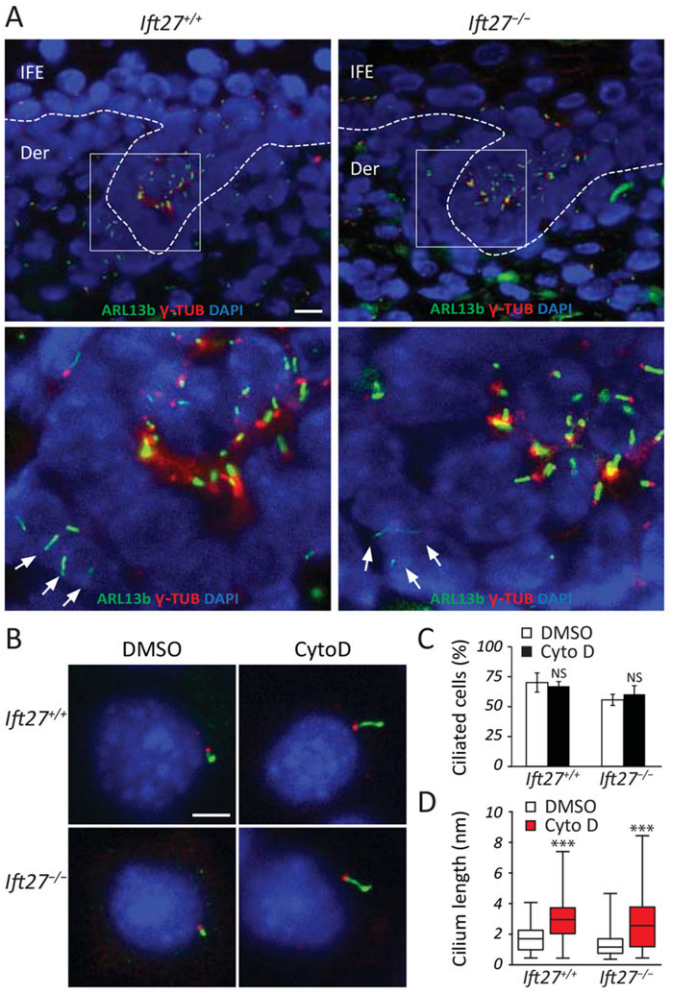

Fig. 4. Ciliogenesis is unaffected in *Ift27*$^{-/-}$ skin. (A) Immunofluorescence labeling of cilia and basal body by ARL13B (green) and γ-tubulin (red) in E18.5 *Ift27*$^{+/+}$ and *Ift27*$^{-/-}$ skin. Dashed lines indicate the epidermal-dermal junction. Lower panels are magnifications of the boxed areas above. Arrows point to ciliated dermal papilla cells. (B) Labeling of cilia and basal body (as described in A) in primary keratinocytes after 24 h treatment with DMSO or cyto D (0.5 µM). Three independent experiments were conducted. (C,D) Statistical analyses of the percentage of ciliated cells (C) and of cilium length (D) in the cyto D-treated cells described in B. NS, not significantly different (one-way ANOVA); ***P<0.0001 (Mann-Whitney test). Scale bars: 10 µm in A; 5 µm in B.

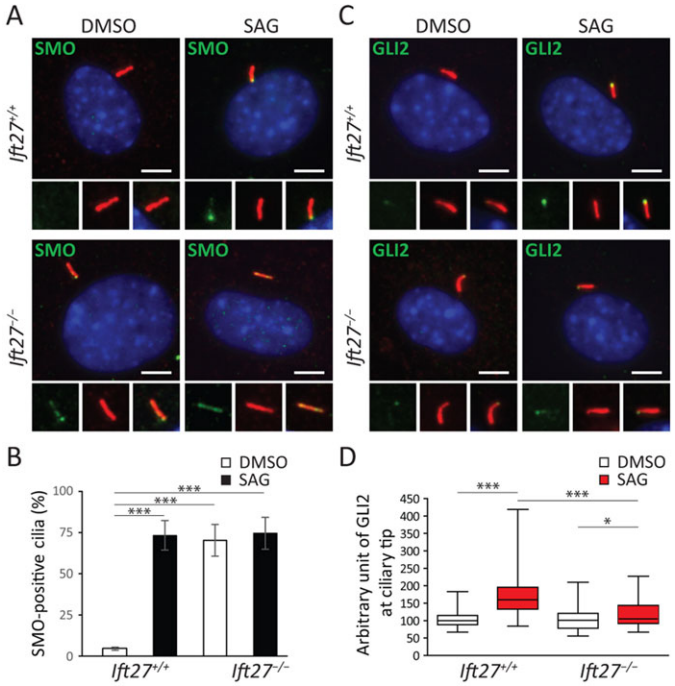

Fig. 5. Localization of SMO and GLI2 in primary cilia. (A) The localization of SMO (green) in control and *Ift27*$^{-/-}$ primary cilia of primary dermal fibroblasts before and after Hh pathway activation (DMSO or SAG treatment, respectively). Primary cilia were labeled by acetylated α-tubulin (red). (B) Statistical analysis of SMO^{+} primary cilia. (C) The localization of GLI2 (green) in primary cilia of primary dermal fibroblasts as shown in A. (A,C) Signals in single and merged channels are shown beneath main images. (D) Statistical analysis of intensity of GLI2 at the ciliary tip. n>125. *P<0.05, ***P<0.001 (one-way ANOVA). Scale bars: 5 µm.

in vitro (Figs 5 and 6). In control dermal fibroblasts, SMO is essentially undetectable in the ciliary axoneme when the Hh pathway in inactive (cells treated with DMSO, Fig. 5A, upper panel). Upon pathway activation (SAG treatment), control cells robustly accumulated SMO in the cilium (Fig. 5A,B). By contrast, SMO abnormally accumulated in cilia of *Ift27*$^{-/-}$ dermal fibroblasts even when the Hh pathway was inactive (Fig. 5A, lower panel). This suggested that the ciliary exit of SMO was defective in *Ift27*$^{-/-}$ cells.

In SAG-treated control fibroblasts GLI2 accumulated at the ciliary tip (Fig. 5C,D), which was consistent with an activated Hh pathway as documented previously (Kim et al., 2009). By contrast, ciliary tip accumulation of GLI2 was severely disrupted in SAG-treated *Ift27*$^{-/-}$ dermal fibroblast (Fig. 5C,D). This result was not only consistent with the suppressed Hh pathway observed *in vivo* and *in vitro* (Fig. 3) but also suggested defective trafficking of Hh components in *Ift27*$^{-/-}$ cells in response to Hh pathway activation.

IFT27 and the expression and localization of other IFT proteins

Since the loss of *Ift27* does not seem to impact ciliogenesis, we further determined whether the expression and ciliary localization of known ciliogenic IFT proteins are affected in *Ift27*$^{-/-}$ cells. First, double immunofluorescence labeling and western blotting confirmed the loss of expression and of the ciliary localization of IFT27 in *Ift27*$^{-/-}$ cells (Fig. 6A,E). Subsequently, we found that the expression patterns of IFT88 and IFT140, which belong to the IFT-B and IFT-A complexes, respectively, were unaffected in *Ift27*$^{-/-}$ cells (Fig. 6C,D). Specifically, IFT88 was enriched in the axoneme and basal body, whereas IFT140 was predominantly localized at the basal body (Fig. 6C,D). The expression level of IFT140 was unchanged in *Ift27*$^{-/-}$ cells as confirmed by western blotting (Fig. 6E). By contrast, in *Ift27*$^{-/-}$ cells the ciliary localization of IFT25 was essentially undetectable (Fig. 6B) and its expression was significantly reduced by 35% (Fig. 6E,F). These data suggested that IFT27 is not required for the expression and localization of IFT proteins that are involved in cilia formation but selectively regulates the stability and localization of its binding partner IFT25, which is also dispensable during cilia formation.

Ift25 mutants phenocopy the hair follicle phenotypes of *Ift27*$^{-/-}$ mice

To confirm the functional relevance of IFT25 during hair follicle formation, we examined the skin of *Ift25*-null (*Ift25*$^{-/-}$) mice (Keady et al., 2012). As expected, *Ift25*$^{-/-}$ mice displayed a hair follicle phenotype almost identical to that of *Ift27*$^{-/-}$ mice (Fig. 7A). Specifically, although the total number of hair follicles remained unaffected (Fig. 7B), the hair follicles of E18.5 *Ift25*$^{-/-}$ embryos

Development (2015) 142, 2194-2202 doi:10.1242/dev.115261

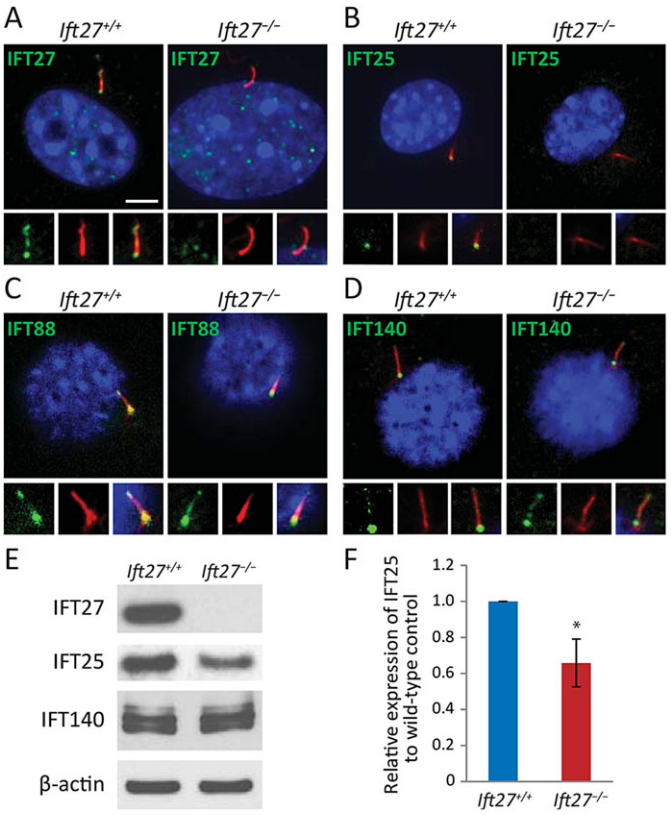

Fig. 6. Distribution of IFT-B and IFT-A proteins in *Ift27*$^{-/-}$ cells. (A-D) The expression of IFT27 (A), IFT25 (B), IFT88 (C) and IFT140 (D) in *Ift27*$^{+/+}$ and *Ift27*$^{-/-}$ primary dermal fibroblasts by colabeling by acetylated α-tubulin (red). Ciliary localization is shown in single channel and merged. (E) Expression levels of IFT27, IFT25 and IFT140 in dermal fibroblasts by western blotting; *n*=3. (F) Quantification of IFT25 as shown in E. The IFT25 protein level was significantly reduced in *Ift27*$^{-/-}$ primary dermal fibroblasts. **P*<0.05. Scale bar: 5 µm.

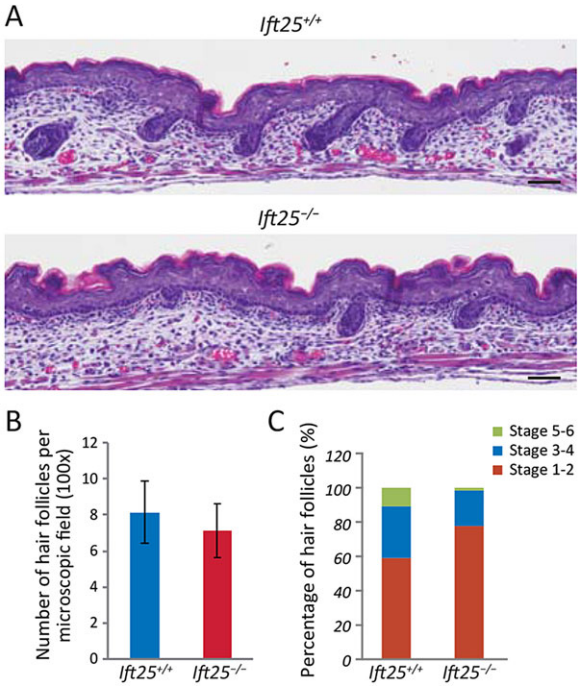

Fig. 7. *Ift25*$^{-/-}$ embryos display defective hair follicle development similar to *Ift27*$^{-/-}$. (A) H&E staining of E18.5 *Ift25*$^{+/+}$ and *Ift25*$^{-/-}$ dorsal skin. (B) Statistical analysis of the number of hair follicles in the dorsal skin of E18.5 *Ift25*$^{+/+}$ and *Ift25*$^{-/-}$ embryos per microscopy field (100×); *n*=4. (C) Distribution of developmental stages of hair follicles of E18.5 dorsal skin. A minimum of 100 hair follicles were analyzed. Scale bars: 100 µm.

displayed severe developmental delay (Fig. 7A,C; $P<0.01$, two-way ANOVA). These data suggested that *Ift27* and *Ift25* engage in a functional association during hair follicle morphogenesis.

DISCUSSION

Hedgehog signaling is required for the crosstalk between follicular keratinocytes and dermal papilla cells during hair follicle development. Activation of the Hh signaling pathway requires the primary cilia. A number of recent studies unequivocally demonstrated that the primary cilium is essential for hair follicle morphogenesis; disrupting ciliogenesis results in the arrest of hair follicle development due to disrupted Hh signaling (Chen et al., 2015; Dai et al., 2013, 2011; Lehman et al., 2009). Thus, the formation of the ciliary axoneme is prerequisite for its function; disrupting cilia formation inevitably disrupts its function, including the transduction of Hh signals. In the current study, we further dissected the ciliogenic processes in the context of hair follicle morphogenesis, and discovered that a subset of IFT proteins, specifically IFT27 and IFT25, are not required for the formation and maintenance of the ciliary axoneme but are essential for processing Hh signaling components. These findings demonstrate that the processes required for transducing the Hh signals may be separated from those of ciliogenesis, and that the presence of the ciliary axoneme does not necessarily warrant functionality.

Ift27$^{-/-}$ and *Ift25*$^{-/-}$ mice die shortly after birth due to severe developmental abnormalities in vital organs, such as the heart, spinal cord and lung (Eguether et al., 2014; Keady et al., 2012). These developmental anomalies were linked to disrupted Hh signaling (Eguether et al., 2014; Keady et al., 2012). The extensive phenotypic outcome in *Ift27*$^{-/-}$ and *Ift25*$^{-/-}$ mice suggests that this subset of IFT proteins might be widely required in the embryonic development of complex organ systems. The recent identification of a loss-of-function mutation in *IFT27* (C99Y) in Bardet-Biedl syndrome (BBS) demonstrated that IFT27 indeed plays an important role in human development and health (Aldahmesh et al., 2014).

The hair follicle phenotype observed in the germline mutant *Ift27*$^{-/-}$ mice is reminiscent of that previously reported for Hh and primary cilia germline mutants (Chen et al., 2015; Chiang et al., 1999; Dai et al., 2011; Gat et al., 1998; Mill et al., 2003; St-Jacques et al., 1998; Woo et al., 2012). Interestingly, when Hh or ciliary genes were disrupted in a tissue-specific fashion, i.e. in the epidermal lineage (Dai et al., 2013) or in mesenchymal cells (Lehman et al., 2009; Woo et al., 2012), the resultant phenotypes were almost identical to those in germline mutants (Chen et al., 2015; Chiang et al., 1999; Dai et al., 2011; Gat et al., 1998; Mill et al., 2003; St-Jacques et al., 1998; Woo et al., 2012). These findings strongly suggest that disrupting Hh signaling or cilia formation/function in either or both tissue compartments of the hair follicle will, individually or collectively, contribute to hair follicle morphogenesis defects.

IFT27 and IFT25 are subunits of the IFT-B complex (Follit et al., 2009; Rosenbaum and Witman, 2002). Direct interactions between these two proteins have been demonstrated previously (Bhogaraju et al., 2011; Keady et al., 2012; Wang et al., 2009b). In this study, we further demonstrated that the stability and subcellular localization of these proteins are required for the morphogenesis of hair follicles, such that disrupting the expression of either of them

Development (2015) 142, 2194-2202 doi:10.1242/dev.115261

could result in hair follicle morphogenesis arrest. It is worth noting that the *Ift25* and *Ift27* mutant mice were able to survive to term, whereas other IFT-B mutants, such as *Ift88*^{fxo}, are unable to survive beyond mid-gestation (Huangfu et al., 2003). The relatively mild phenotypes in the former suggested that IFT25 and IFT27 might have more restricted functions, such as in transducing Hh signals as shown herein, in comparison to IFT88, which is essential for ciliogenesis in a wide range of cell types. Interestingly, disrupting *Ift88* resulted in similar hair follicle phenotypes (Lehman et al., 2009) to those of the *Ift25* and *Ift27* mutants described herein. Because these hair follicle phenotypes were attributed to attenuated Hh signaling, these studies collectively suggest that the core function of primary cilia during hair follicle morphogenesis is the transduction of Hh signals.

The ciliogenic capability of *Ift27*$^{-/-}$ cells was further examined using cyto D, which is capable of elongating the ciliary axoneme. *Ift27*$^{-/-}$ dermal fibroblasts treated with cyto D showed a comparable capacity to elongate the ciliary axoneme as control cells. Similarly, neither the expression nor localization of known ciliogenic IFT proteins, such as IFT88 and IFT140, nor the trafficking of ciliary membrane-associated proteins, such as ARL13B and ADCY3, was affected in *Ift27*$^{-/-}$ cells. These data suggested that *Ift27* is not involved in the machinery required for ciliary length maintenance nor the trafficking of key ciliogenic proteins in mammalian cells. A recent study on the flagellum of *Trypanosoma brucei* suggested that IFT27 is involved in both anterograde and retrograde trafficking (Huet et al., 2014). Whether IFT27 performs cellular functions beyond trafficking Hh components remains to be determined in mammalian cells.

IFT27 was recently shown to play a crucial role in facilitating ciliary exit of the BBSome (Eguether et al., 2014; Ng et al., 2012), and *Ift27*-deficient mouse embryonic fibroblasts are unable to maintain low levels of SMO in the cilia when the Hh pathway is inactive (Eguether et al., 2014). In this study, we further demonstrated that suppressed Hh signaling in *Ift27*$^{-/-}$ primary dermal fibroblasts is also associated with abnormal accumulation of SMO in the cilium. However, ciliary accumulation of SMO does not necessarily correlate with pathway activation (Rohatgi et al., 2009). Thus, data obtained in this study suggest that disrupted Hh signaling in *Ift27*$^{-/-}$ cells may be associated with abnormal trafficking of Hh pathway components in the primary cilium.

The primary cilium is essential for the processing of Gli transcription factors. It is well documented that in the absence of Hh ligands GLI3-FL is processed to its repressor form GLI3-R, resulting in a relatively low GLI3-FL:GLI3-R ratio (Niewiadomski et al., 2014). Data obtained from this study demonstrated that disrupting *Ift27* results in an attenuated Hh pathway and, counterintuitively, an elevated GLI3-FL level, suppressed GLI3-R level, and increased GLI3-FL:GLI3-R ratio. We speculate that these changes in *Ift27*$^{-/-}$ cells do not necessarily correspond to activation of the Hh pathway. Rather, they might merely reflect that IFT27 is required for proper processing of GLI3-FL. These data are in line with the well-documented observation that ligand-induced activation of the Hh pathway, and thus the production of Gli activators (but not GLI3-R), plays a predominant role during hair follicle morphogenesis (Mill et al., 2003). Thus, despite the elevated GLI3-FL level or increased GLI3-FL:GLI3-R ratio, the net outcome of disrupting *Ift27* is Hh pathway suppression and impaired hair follicle morphogenesis. Moreover, Hh pathway activity is modulated by multiple phosphorylations of Gli transcription factors (both activators and suppressors) (Niewiadomski et al., 2014). Thus, data obtained from this study support the notion that Hh pathway activity may not be evaluated simplistically based on the levels of Gli transcription factors, and that precisely controlled processing of Gli transcription factors is an integral component of the Hh signaling pathway.

By examining key events associated with skin and hair follicle morphogenesis, we noticed that the effect of loss of *Ift27* was restricted to the proliferation and cytodifferentiation of follicular keratinocytes. Stratification, proliferation and differentiation of the interfollicular epidermis and the induction of hair germ were unaffected in *Ift27*$^{-/-}$ mutants. These phenotypes correlated well with related molecular signaling pathways, such as attenuated Hh signaling and relatively normal canonical Wnt, Notch, BMP and TGFβ signaling in *Ift27*$^{-/-}$ skin. Thus, the cell fate-specific function of IFT27 can be attributed primarily to its function in processing Hh signals. Whether IFT27 participates in the transduction of other molecular signals in the skin remains to be empirically determined.

In summary, this study demonstrated an essential role of *Ift27* in mediating Hh signaling during follicular keratinocyte proliferation and differentiation but not the differentiation program of the interfollicular epidermis. Although the full spectrum of *Ift27* functions remains to be uncovered, the rather restricted function of IFT27 during embryonic skin development provides important insight into a novel avenue of targeting Hh signaling, such as in the targeted therapy for basal cell carcinoma (BCC), in which tumors not only originate from the hair follicles but are also dependent on hyperactive Hh signaling (Epstein, 2008; Kasper et al., 2012). Because IFT27 is likely to mediate Hh signaling through regulating the ciliary localization of SMO and the processing of Gli transcription factors, targeting IFT27 might prevent the development of drug resistance caused by acquired mutations in the SMO receptor following Vismodegib treatment (Yauch et al., 2009).

MATERIALS AND METHODS

Generation of *Ift27*$^{-/-}$ mice and skin transplantation

Ift27-targeted embryonic stem cells [*Ift27*$^{tm1a(EUCOMM)Hmgu}$] were obtained from the EUCOMM project and used to create *Ift27* mutant mice (Eguether et al., 2014). Homozygous mutants were obtained by crossing *Ift27*$^{+/-}$ mice. Genotypes of *Ift27* mutants were determined using the following primer pairs (5′-3′): F, GGGAGATGAGGGATTCTTCC; R1, TCCAACTCTGACTCCGTCCT; R2, CCCCCTGAACCTGAAACATA. E15.5 and E18.5 embryos were obtained by timed mating. Full-thickness skin transplantation was performed as previously described (Dai et al., 2011). All procedures related to mice were approved by the IACUC of the University of Massachusetts Medical School and Stony Brook University.

BrdU labeling and tissue processing

Bromodeoxyuridine (BrdU) labeling was performed by intraperitoneally injecting 10 µg BrdU labeling reagent (Invitrogen) per gram body weight 2 hours prior to euthanasia. Skin specimens were obtained by removing the full-thickness dorsal skin with surgical tools and were fixed in 10% buffered formalin at 4°C overnight. Fixed skin specimens were processed and sectioned for routine histology analysis. For all analyses, a minimum of three embryos obtained from at least two different litters were examined. AP staining was performed as previously described (Tsai et al., 2010). Specifically, frozen skin sections were fixed in 4% paraformaldehyde, soaked in B3 buffer (0.1 M Tris pH 9.5, 0.1 M NaCl, 0.05 M $MgCl_2$) for 10 min, then in NBT (1:200)/BCIP (1:267) solution (Roche) for 20 min, and imaged.

Cell culture and *in vitro* assays

The isolation of primary skin keratinocytes and dermal fibroblasts was conducted as described (Marshall et al., 2005). Briefly, E18.5 skin was digested by dispase II (Roche) to separate epidermis and dermis. Epidermis or dermis was then digested with trypsin or collagenase, respectively, to collect keratinocytes and dermal fibroblasts. Cells were used directly for

Development (2015) 142, 2194-2202 doi:10.1242/dev.115261

skin reconstitution or cultured *in vitro*. Keratinocytes were cultured in defined keratinocyte serum-free medium (Life Technologies) on collagen I-coated tissue culture plates. Fibroblasts were cultured in Dulbecco's modified Eagle's medium (4.5 g/l glucose) supplemented with 10% fetal bovine serum and 100 U/ml penicillin and 100 U/ml streptomycin. To examine cilia formation, cells were grown to near confluence and serum starved for 24 h before being treated with SAG (100 nM, Calbiochem) or cyto D (0.5 µM, Sigma) for an additional 24 h in serum-free medium.

Quantitative RT-PCR and western blotting

RNA isolation and quantitative RT-PCR analyses were performed as described previously (Dai et al., 2013). The following probes were used for TaqMan analysis: *Ift27*, ABI Mm00508912_m1; *Ptch1*, Mm00436026_m1; *Gli1*, Mm00494645_m1; *Gli2*, Mm01293111_m1; *Smo*, Mm01162710_m1; and *Actb*, Mm00607939_m1 (Life Technologies). Results were analyzed using the ΔΔCt method. Relative expression levels of target genes were determined by comparison with wild-type or treatment controls after normalizing to β-actin.

Protein was extracted either by homogenizing skin in cold RIPA lysis buffer (1% Triton X-100, 0.1% SDS, 50 mM Tris-HCl pH 7.4, 150 mM NaCl, 1% sodium deoxycholate, 2 mM EDTA, 50 mM NaF) supplemented with proteinase inhibitors or by digesting cells directly in RIPA lysis buffer. Cell lysates were cleared by centrifugation at 13,000 ***g*** for 20 min at 4°C; protein concentration was determined using the BCA Protein Assay Kit (Pierce). Nuclear fractionation was conducted with the NE-PER Nuclear and Cytoplasmic Extraction Kit (Thermo Scientific). Proteins were separated on a NuPage gel (Life Technologies) and transferred to Hybond nitrocellulose membranes (GE Healthcare). The following primary antibodies were used: β-actin (1:1000; Santa Cruz, sc-47778), IFT27 [1:1000; gift of G. Pazour, University of Massachusetts (Keady et al., 2012)], GLI1 (1:250; clone V812, Cell Signaling, 2534S), GLI3 (1:200; R&D Systems, AF3690), IFT25 (1:1000; Proteintech, 15732-1-AP) and IFT140 [1:500 (Uitto, 2012)]. HRP-conjugated secondary antibodies (BD Biosciences), SuperSignal substrates (Thermo Scientific) and CL-XPosure film (Thermo Scientific) were used for detection. Quantification of signal was performed with ImageJ (NIH).

Immunofluorescence labeling and microscopy

Immunofluorescence labeling was performed as described previously (Dai et al., 2013). The following primary antibodies were used: TRP63 (1:100; Santa Cruz Biotechnology, sc-8431), KRT14 [1:1000 (Roop et al., 1987)], KRT1 [1:500 (Roop et al., 1987)], KRT17 (1:400; Abcam, ab111446), LOR [1:100 (Roop et al., 1987)], LEF1 (1:100; Cell Signaling, 2230), NGFR (1:200; $p75^{NTR}$, Promega, G3231), BrdU (1:20; Life Technologies, A21304), acetylated α-tubulin (1:1000; Sigma, T6793), γ-tubulin (1:500; Abcam, ab11317 and ab11316), ARL13B (1:100; NeuroMab, #73-287), IFT27 and IFT140 [1:200 (Keady et al., 2012)], IFT25 (1:200; Proteintech, 15732-1-AP), IFT88 (1:600; Proteintech, 23967-1-AP), SMO [1:100; gift of R. Rohatgi, Stanford University (Rohatgi et al., 2007)], GLI2 [1:1000; gift of J. Eggenschwiler, University of Georgia (Sperling et al., 2010)], pSMAD1/5 (1:100; Cell Signaling, 9511s) and pSMAD2 (1:100; Cell Signaling, 3101). Alexa Fluor-conjugated secondary antibodies (1:250) were from Life Technologies. Sections were sealed in mounting medium with DAPI (Vector Laboratories). Images were acquired using a Nikon 80i fitted with a Nikon DS-Qi1Mc camera and processed with Photoshop 5.5 CS (Adobe).

To quantify GLI2 at the ciliary tip, GLI2 fluorescence intensity in a defined circular area (comprising 100 pixels) at the distal end of each cilium was measured using ImageJ. Intensity was normalized as percentage of the median intensity of the wild-type control group. A minimum of 125 cilia from three sets of wild-type and $Ift27^{-/-}$ primary dermal fibroblasts were evaluated.

In situ hybridization

In situ hybridization was carried out on formalin-fixed paraffin-embedded tissue sections using RNAScope *in situ* hybridization technology [Advanced Cell Diagnostics (Wang et al., 2012)] and custom mouse *Ift27*, *Gli1*, *Ptch1* and *Shh* probes as per the manufacturer's instructions.

Scanning electron microscopy (SEM)

For SEM of cilia, primary keratinocytes isolated from E18.5 mice were fixed overnight in 2.5% glutaraldehyde in 0.1 M phosphate buffer (pH 7.4). Cells were then post-fixed, dehydrated and gold coated through standard procedures (Bechtold, 2000). Samples were examined on a JOEL S-3000N scanning electron microscope (Hitachi).

Statistical analyses

All quantifications are presented as mean±s.d. Student's *t*-test was used unless stated otherwise. One-way ANOVA and two-way ANOVA were conducted using GraphPad Prism. $P<0.05$ was considered statistically significant.

Acknowledgements

We thank Mallory Korman and Kathleen Silva for assistance in histological sample processing; Laurie Levine for assistance with experimental animals; Christy Ou for assistance with experiments and data analysis; Yeun Ja Choi and Elizabeth Snedecor for discussion; and Dr Tamara Caspary for providing the ARL13B antibody.

Competing interests

The authors declare no competing or financial interests.

Author contributions

N.Y., J.P.S., G.J.P. and J.C. designed experiments and analyzed data. L.L. and T.E. performed preliminary experiments. N.Y. and J.C. carried out the experiments, collected the data and wrote the manuscript.

Funding

This study was supported by grants from the International Union Against Cancer (UICC) and American Cancer Society (ACS) Beginning Investigators to L.L., a P&F grant from the Skin Disease Research Center (SDRC) of the University of Colorado Denver, start-up funds provided by the Department of Pathology and the Cancer Center of Stony Brook University, and research grants from the National Institutes of Health [R061485 to J.C., AR063781 to J.P.S. and GM060992 to G.J.P.]. Deposited in PMC for release after 12 months.

Supplementary material

Supplementary material available online at
http://dev.biologists.org/lookup/suppl/doi:10.1242/dev.115261/-/DC1

References

Aldahmesh, M. A., Li, Y., Alhashem, A., Anazi, S., Alkuraya, H., Hashem, M., Awaji, A. A., Sogaty, S., Alkharashi, A., Alzahrani, S. et al. (2014). IFT27, encoding a small GTPase component of IFT particles, is mutated in a consanguineous family with Bardet-Biedl syndrome. *Hum. Mol. Genet.* **23**, 3307-3315.

Bechtold, L. S. (2000). Ultrastructural evaluation of mouse mutations. In *Systematic Characterization of Mouse Mutations* (ed. J. P. Sundberg and D. Boggess), pp. 121-129. Boca Raton: CRC Press.

Bhogaraju, S., Taschner, M., Morawetz, M., Basquin, C. and Lorentzen, E. (2011). Crystal structure of the intraflagellar transport complex 25/27. *EMBO J.* **30**, 1907-1918.

Blanpain, C., Lowry, W. E., Pasolli, H. A. and Fuchs, E. (2006). Canonical notch signaling functions as a commitment switch in the epidermal lineage. *Genes Dev.* **20**, 3022-3035.

Candi, E., Dinsdale, D., Rufini, A., Salomoni, P., Knight, R. A., Mueller, M., Krammer, P. H. and Melino, G. (2007). TAp63 and DeltaNp63 in cancer and epidermal development. *Cell Cycle* **6**, 274-284.

Candi, E., Cipollone, R., Rivetti di Val Cervo, P., Gonfloni, S., Melino, G. and Knight, R. (2008). p63 in epithelial development. *Cell. Mol. Life Sci.* **65**, 3126-3133.

Chen, J., Laclef, C., Moncayo, A., Snedecor, E. R., Yang, N., Li, L., Takemaru, K.-I., Paus, R., Schneider-Maunoury, S. and Clark, R. A. (2015). The ciliopathy gene Rpgrip1l is essential for hair follicle development. *J. Investig. Dermatol.* **135**, 701-709.

Chiang, C., Swan, R. Z., Grachtchouk, M., Bolinger, M., Litingtung, Y., Robertson, E. K., Cooper, M. K., Gaffield, W., Westphal, H., Beachy, P. A. et al. (1999). Essential role for Sonic hedgehog during hair follicle morphogenesis. *Dev. Biol.* **205**, 1-9.

Cole, D. G. (2003). The intraflagellar transport machinery of Chlamydomonas reinhardtii. *Traffic* **4**, 435-442.

Cole, D. G. and Snell, W. J. (2009). SnapShot: intraflagellar transport. *Cell* **137**, 784-784.e1.

Cole, D. G., Diener, D. R., Himelblau, A. L., Beech, P. L., Fuster, J. C. and Rosenbaum, J. L. (1998). Chlamydomonas kinesin-II-dependent intraflagellar

transport (IFT): IFT particles contain proteins required for ciliary assembly in Caenorhabditis elegans sensory neurons. *J. Cell Biol.* **141**, 993-1008.
Corbit, K. C., Aanstad, P., Singla, V., Norman, A. R., Stainier, D. Y. R. and Reiter, J. F. (2005). Vertebrate Smoothened functions at the primary cilium. *Nature* **437**, 1018-1021.
Dai, D., Zhu, H., Wlodarczyk, B., Zhang, L., Li, L., Li, A. G., Finnell, R. H., Roop, D. R. and Chen, J. (2011). Fuz controls the morphogenesis and differentiation of hair follicles through the formation of primary cilia. *J. Investig. Dermatol.* **131**, 302-310.
Dai, D., Li, L., Huebner, A., Zeng, H., Guevara, E., Claypool, D. J., Liu, A. and Chen, J. (2013). Planar cell polarity effector gene Intu regulates cell fate-specific differentiation of keratinocytes through the primary cilia. *Cell Death Differ.* **20**, 130-138.
Eguether, T., San Agustin, J. T., Keady, B. T., Jonassen, J. A., Liang, Y., Francis, R., Tobita, K., Johnson, C. A., Abdelhamed, Z. A., Lo, C. W. et al. (2014). IFT27 links the BBSome to IFT for maintenance of the ciliary signaling compartment. *Dev. Cell* **31**, 279-290.
Epstein, E. H. (2008). Basal cell carcinomas: attack of the hedgehog. *Nat. Rev. Cancer* **8**, 743-754.
Follit, J. A., Xu, F., Keady, B. T. and Pazour, G. J. (2009). Characterization of mouse IFT complex B. *Cell Motil. Cytoskeleton* **66**, 457-468.
Gat, U., DasGupta, R., Degenstein, L. and Fuchs, E. (1998). De Novo hair follicle morphogenesis and hair tumors in mice expressing a truncated beta-catenin in skin. *Cell* **95**, 605-614.
Haycraft, C. J., Banizs, B., Aydin-Son, Y., Zhang, Q., Michaud, E. J. and Yoder, B. K. (2005). Gli2 and Gli3 localize to cilia and require the intraflagellar transport protein polaris for processing and function. *PLoS Genet.* **1**, e53.
Houde, C., Dickinson, R. J., Houtzager, V. M., Cullum, R., Montpetit, R., Metzler, M., Simpson, E. M., Roy, S., Hayden, M. R., Hoodless, P. A. et al. (2006). Hippi is essential for node cilia assembly and Sonic hedgehog signaling. *Dev. Biol.* **300**, 523-533.
Huangfu, D. and Anderson, K. V. (2005). Cilia and Hedgehog responsiveness in the mouse. *Proc. Natl. Acad. Sci. USA* **102**, 11325-11330.
Huangfu, D., Liu, A., Rakeman, A. S., Murcia, N. S., Niswander, L. and Anderson, K. V. (2003). Hedgehog signalling in the mouse requires intraflagellar transport proteins. *Nature* **426**, 83-87.
Huet, D., Blisnick, T., Perrot, S. and Bastin, P. (2014). The GTPase IFT27 is involved in both anterograde and retrograde intraflagellar transport. *Elife* **3**, e02419.
Kasper, M., Jaks, V., Hohl, D. and Toftgård, R. (2012). Basal cell carcinoma — molecular biology and potential new therapies. *J. Clin. Invest.* **122**, 455-463.
Keady, B. T., Samtani, R., Tobita, K., Tsuchya, M., San Agustin, J. T., Follit, J. A., Jonassen, J. A., Subramanian, R., Lo, C. W. and Pazour, G. J. (2012). IFT25 links the signal-dependent movement of Hedgehog components to intraflagellar transport. *Dev. Cell* **22**, 940-951.
Kim, J., Kato, M. and Beachy, P. A. (2009). Gli2 trafficking links Hedgehog-dependent activation of Smoothened in the primary cilium to transcriptional activation in the nucleus. *Proc. Natl. Acad. Sci. USA* **106**, 21666-21671.
Kozminski, K. G., Johnson, K. A., Forscher, P. and Rosenbaum, J. L. (1993). A motility in the eukaryotic flagellum unrelated to flagellar beating. *Proc. Natl. Acad. Sci. USA* **90**, 5519-5523.
Lehman, J. M., Laag, E., Michaud, E. J. and Yoder, B. K. (2009). An essential role for dermal primary cilia in hair follicle morphogenesis. *J. Investig. Dermatol.* **129**, 438-448.
Marshall, W. F., Qin, H., Rodrigo Brenni, M. and Rosenbaum, J. L. (2005). Flagellar length control system: testing a simple model based on intraflagellar transport and turnover. *Mol. Biol. Cell* **16**, 270-278.
Mill, P., Mo, R., Fu, H., Grachtchouk, M., Kim, P. C. W., Dlugosz, A. A. and Hui, C.-C. (2003). Sonic hedgehog-dependent activation of Gli2 is essential for embryonic hair follicle development. *Genes Dev.* **17**, 282-294.
Ng, C. S., Wu, P., Foley, J., Foley, A., McDonald, M.-L., Juan, W.-T., Huang, C.-J., Lai, Y.-T., Lo, W.-S., Chen, C.-F. et al. (2012). The chicken frizzle feather is due to an alpha-keratin (KRT75) mutation that causes a defective rachis. *PLoS Genet.* **8**, e1002748.
Niewiadomski, P., Kong, J. H., Ahrends, R., Ma, Y., Humke, E. W., Khan, S., Teruel, M. N., Novitch, B. G. and Rohatgi, R. (2014). Gli protein activity is controlled by multisite phosphorylation in vertebrate Hedgehog signaling. *Cell Rep.* **6**, 168-181.
Paus, R., Müller-Röver, S., van Der Veen, C., Maurer, M., Eichmüller, S., Ling, G., Hofmann, U., Foitzik, K., Mecklenburg, L. and Handjiski, B. (1999). A comprehensive guide for the recognition and classification of distinct stages of hair follicle morphogenesis. *J. Investig. Dermatol.* **113**, 523-532.
Qin, H., Wang, Z., Diener, D. and Rosenbaum, J. (2007). Intraflagellar transport protein 27 is a small G protein involved in cell-cycle control. *Curr. Biol.* **17**, 193-202.
Rohatgi, R., Milenkovic, L. and Scott, M. P. (2007). Patched1 regulates hedgehog signaling at the primary cilium. *Science* **317**, 372-376.
Rohatgi, R., Milenkovic, L., Corcoran, R. B. and Scott, M. P. (2009). Hedgehog signal transduction by Smoothened: pharmacologic evidence for a 2-step activation process. *Proc. Natl. Acad. Sci. USA* **106**, 3196-3201.
Roop, D. R., Huitfeldt, H., Kilkenny, A. and Yuspa, S. H. (1987). Regulated expression of differentiation-associated keratins in cultured epidermal cells detected by monospecific antibodies to unique peptides of mouse epidermal keratins. *Differentiation* **35**, 143-150.
Rosenbaum, J. L. and Witman, G. B. (2002). Intraflagellar transport. *Nat. Rev. Mol. Cell Biol.* **3**, 813-825.
Schmidt-Ullrich, R. and Paus, R. (2005). Molecular principles of hair follicle induction and morphogenesis. *Bioessays* **27**, 247-261.
Sperling, L. C., Hussey, S., Sorrells, T., Wang, J.-a. and Darling, T. (2010). Cytokeratin 75 expression in central, centrifugal, cicatricial alopecia–new observations in normal and diseased hair follicles. *J. Cutan. Pathol.* **37**, 243-248.
St-Jacques, B., Dassule, H. R., Karavanova, I., Botchkarev, V. A., Li, J., Danielian, P. S., McMahon, J. A., Lewis, P. M., Paus, R. and McMahon, A. P. (1998). Sonic hedgehog signaling is essential for hair development. *Curr. Biol.* **8**, 1058-1069.
Tsai, S. Y., Clavel, C., Kim, S., Ang, Y. S., Grisanti, L., Lee, D. F., Kelley, K. and Rendl, M. (2010). Oct4 and klf4 reprogram dermal papilla cells into induced pluripotent stem cells. *Stem Cells* **28**, 221-228.
Tukachinsky, H., Lopez, L. V. and Salic, A. (2010). A mechanism for vertebrate Hedgehog signaling: recruitment to cilia and dissociation of SuFu-Gli protein complexes. *J. Cell Biol.* **191**, 415-428.
Uitto, J. (2012). Molecular therapeutics for heritable skin diseases. *J. Investig. Dermatol.* **132**, E29-E34.
Wang, Y., Zhou, Z., Walsh, C. T. and McMahon, A. P. (2009a). Selective translocation of intracellular Smoothened to the primary cilium in response to Hedgehog pathway modulation. *Proc. Natl. Acad. Sci. USA* **106**, 2623-2628.
Wang, Z., Fan, Z.-C., Williamson, S. M. and Qin, H. (2009b). Intraflagellar transport (IFT) protein IFT25 is a phosphoprotein component of IFT complex B and physically interacts with IFT27 in Chlamydomonas. *PLoS ONE* **4**, e5384.
Wang, F., Flanagan, J., Su, N., Wang, L.-C., Bui, S., Nielson, A., Wu, X., Vo, H.-T., Ma, X.-J. and Luo, Y. (2012). RNAscope: a novel in situ RNA analysis platform for formalin-fixed, paraffin-embedded tissues. *J. Mol. Diagn.* **14**, 22-29.
Wong, S. Y., Seol, A. D., So, P.-L., Ermilov, A. N., Bichakjian, C. K., Epstein, E. H., Jr, Dlugosz, A. A. and Reiter, J. F. (2009). Primary cilia can both mediate and suppress Hedgehog pathway–dependent tumorigenesis. *Nat. Med.* **15**, 1055-1061.
Woo, W.-M., Zhen, H. H. and Oro, A. E. (2012). Shh maintains dermal papilla identity and hair morphogenesis via a Noggin-Shh regulatory loop. *Genes Dev.* **26**, 1235-1246.
Yauch, R. L., Dijkgraaf, G. J. P., Alicke, B., Januario, T., Ahn, C. P., Holcomb, T., Pujara, K., Stinson, J., Callahan, C. A., Tang, T. et al. (2009). Smoothened mutation confers resistance to a Hedgehog pathway inhibitor in medulloblastoma. *Science* **326**, 572-574.

Fig S1

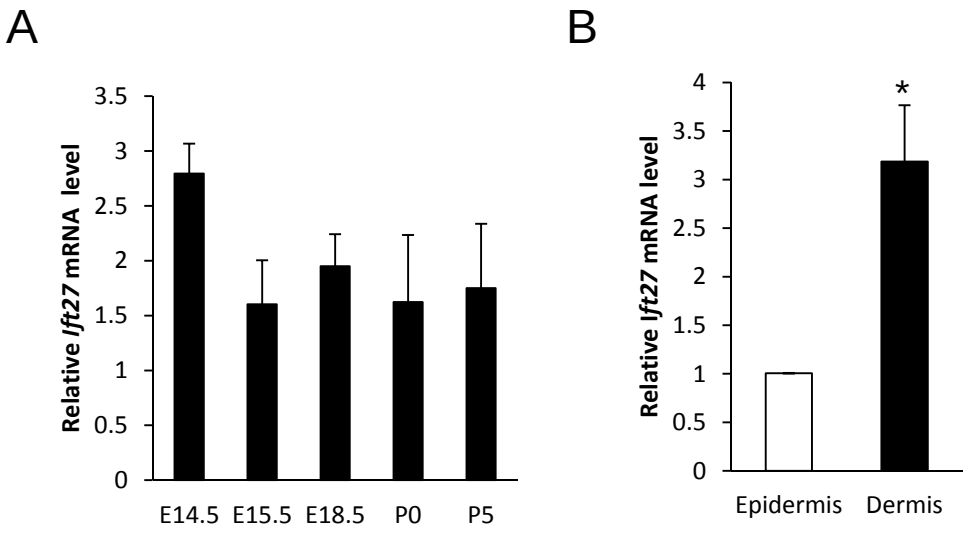

Fig. S1. *Ift27* mRNA expression in mouse skin. (**A**) *Ift27* mRNA level during skin development. n=4. (**B**) *Ift27* mRNA levels in epidermis and dermis of E18.5 embryos. n=3. *, *P*<0.05.

Fig S2

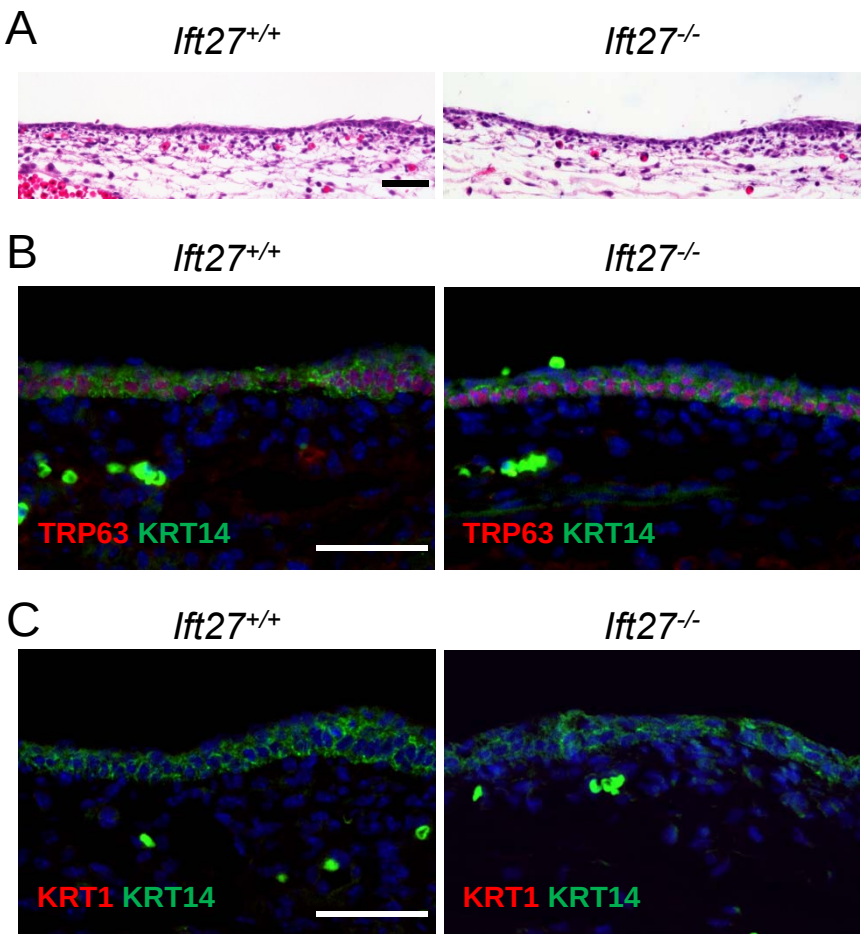

Fig. S2. Control (*Ift27*$^{+/+}$) and *Ift27* mutant (*Ift27*$^{-/-}$) skins at E14.5. (**A**) H&E staining. (**B**) TRP63 (red) and KRT14 (green). (**C**) KRT1 (red) and KRT14 (green). Note, KRT1 is absent. Scale bars: 50 µm.

Fig S3

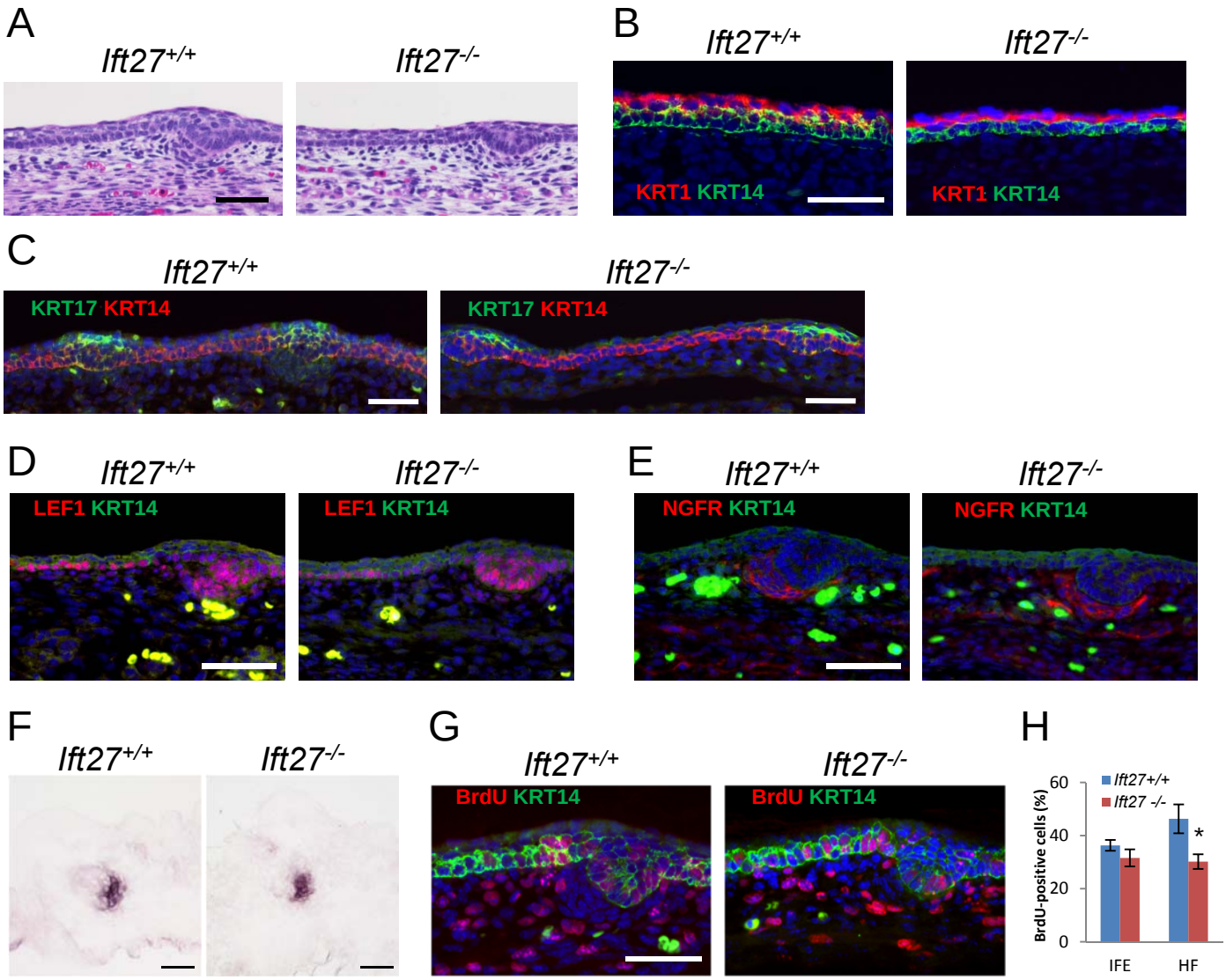

Fig. S3. Control (*Ift27*$^{+/+}$) and *Ift27* mutant (*Ift27*$^{-/-}$) skins at E15.5. (**A**) H&E staining. (**B**) KRT1 (red) and KRT14 (green). (**C**) KRT17 (green) and KRT14 (red). (**D**) LEF1 (red) and KRT14 (green). (**E**), NGFR (p75^{NTR}, red) and KRT14 (green). (**F**) Alkaline phosphatase (AP) staining in E16.5 skins. (**G**) BrdU (red) and KRT14 (green). (**H**) Quantification of BrdU-positive cells in interfollicular epidermis (IFE) and hair follicles (HF). *, *P*<0.05. Scale bars: 50 µm.

Fig S4

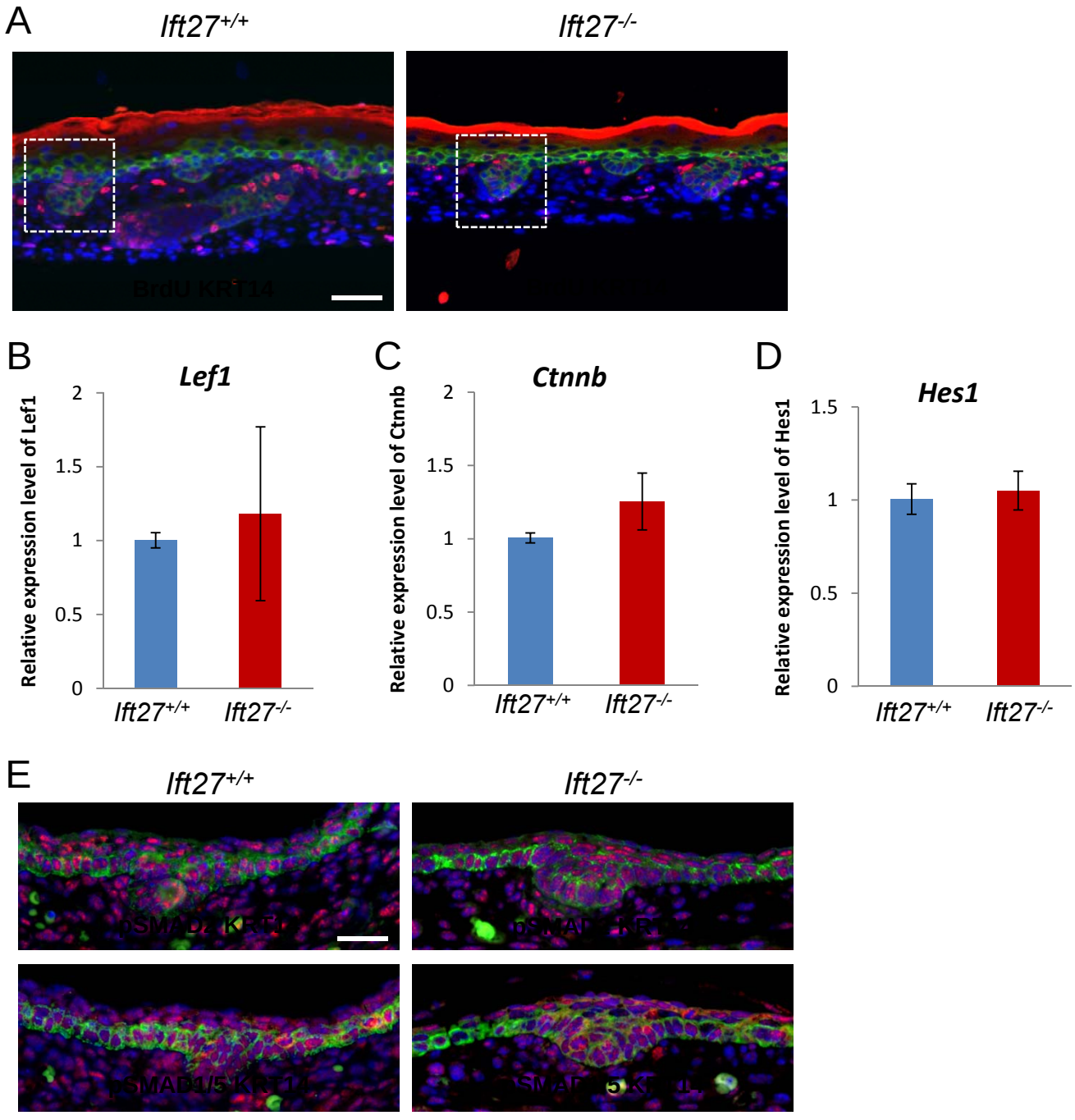

Fig. S4. Control (*Ift27*$^{+/+}$) and *Ift27* mutant (*Ift27*$^{-/-}$) skins at E18.5. (**A**) BrdU (red) and KRT14 (green). Note that BrdU-positive cells in stage 2 hair follicles (boxed) were quantified. (**B**–**D**) Relative expression levels of *Lef1*, *Ctnnb* and *Hes1* by quantitative RT-PCR. Note, the expression levels of these Wnt and Notch target genes are comparable in *Ift27*$^{+/+}$ and *Ift27*$^{-/-}$ skins. n=3. (**E**) Expression of phospho-SMAD2 (pSMAD2) and phospho-SMAD1/5 (pSMAD1/5) in control and mutant skin. Scale bar: 50 µm in A, 25 µm in E.

Fig S5

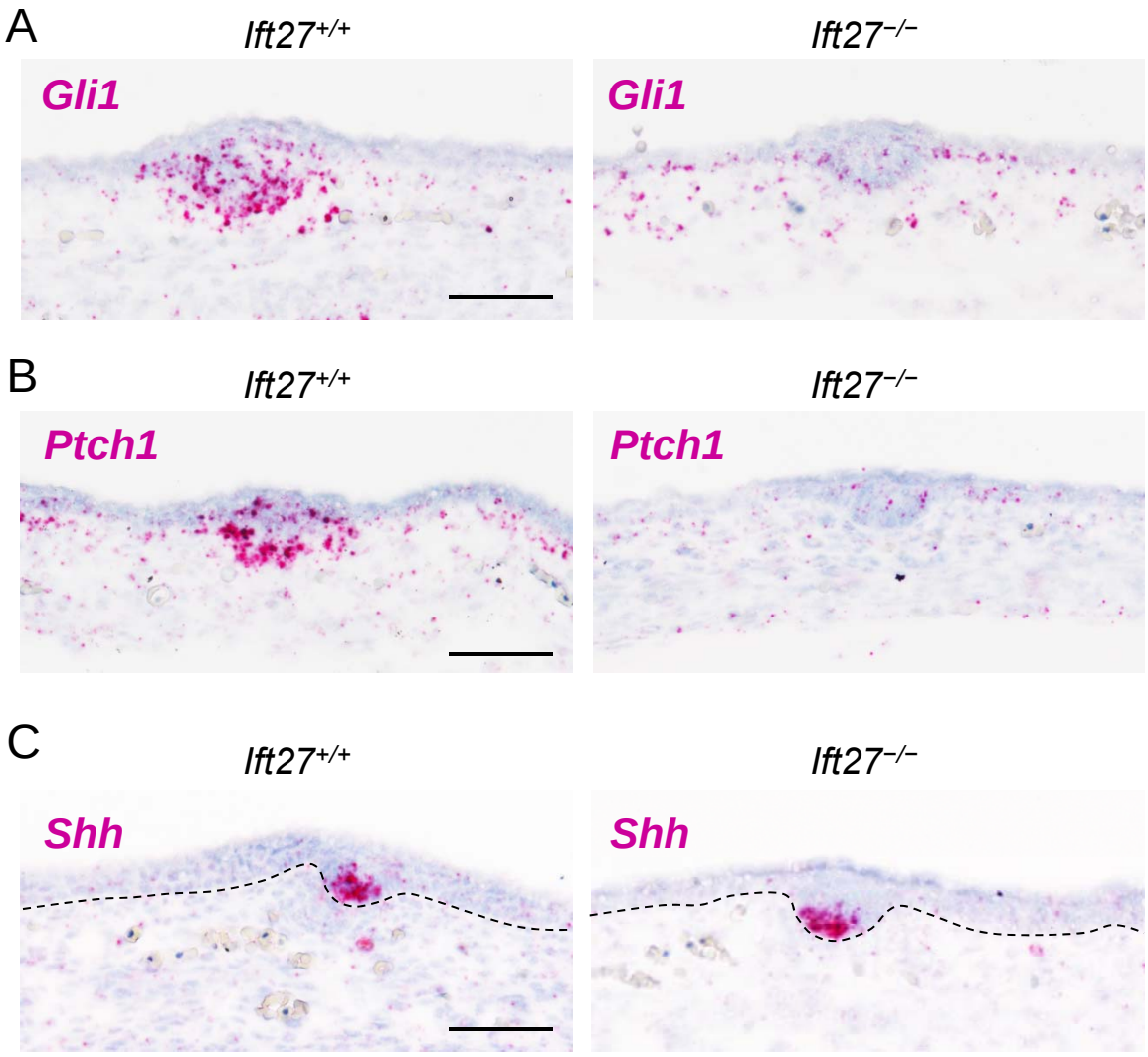

Fig. S5. Hedgehog signaling in skin of E15.5 control (*Ift27*$^{+/+}$) and *Ift27* mutant (*Ift27*$^{-/-}$). (**A**–**C**) *In situ* hybridization of *Gli1* (A), *Ptch1* (B), and *Shh* (C) in E15.5 skins of control and *Ift27* mutant, n=3. Dotted lines represent basement membrane. Note that the expression of *Shh* was comparable in hair follicles of control and *Ift27* mutant. Scale bars: 50 µm.

Fig S6

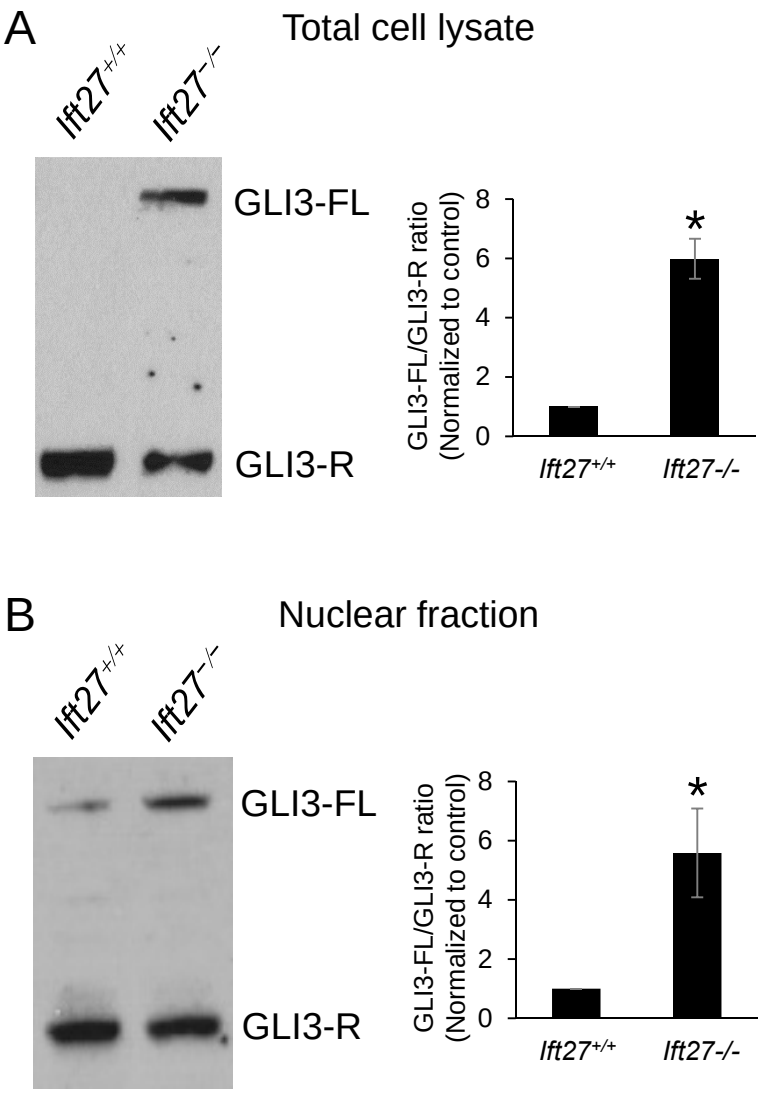

Fig. S6. Expression of full-length GLI3 (GLI3-FL) and repressor form of GLI3 (GLI3-R) in primary dermal fibroblast isolated from control (*Ift27*$^{+/+}$) and *Ift27* mutants (*Ift27*$^{-/-}$). (**A**) Representative western blotting and quantification of GLI3 in whole cell lysate. (**B**) Representative western blotting and quantification of GLI3 in the nuclear fraction of the cells. n=3. *, *P*<0.05.

Fig. S7

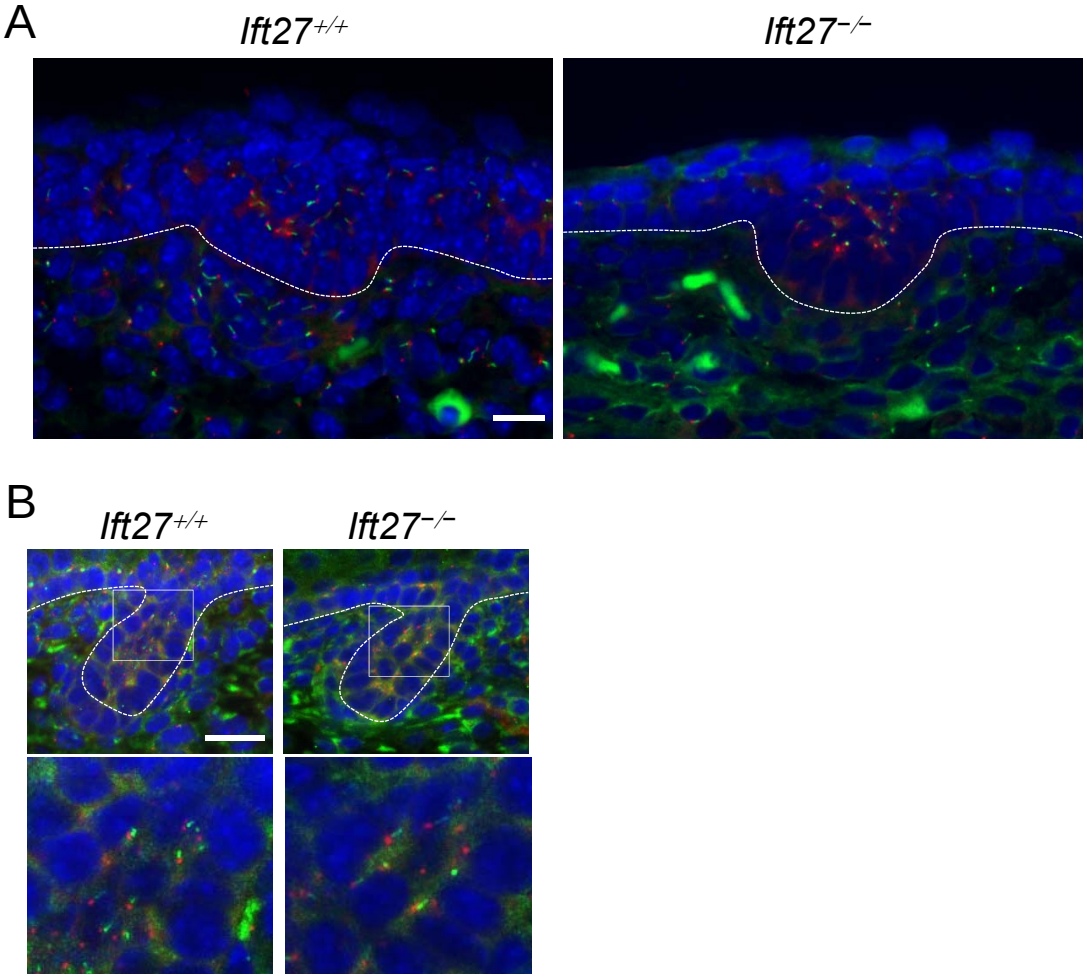

Fig. S7. Primary cilia in control (*Ift27*$^{+/+}$) and *Ift27* mutant (*Ift27*$^{-/-}$). (**A**) Cilia (ARL13B, green) and basal body (γ -tubulin, red) in hair follicles of E15.5 skins. (**B**) Cilia (ACIII, green) and basal body (γ-tubulin, red) in stage 2 hair follicles of E18.5 skins. Lower panels are enlarged boxed areas above. Scale bars: 25 µm.

Fig. S8

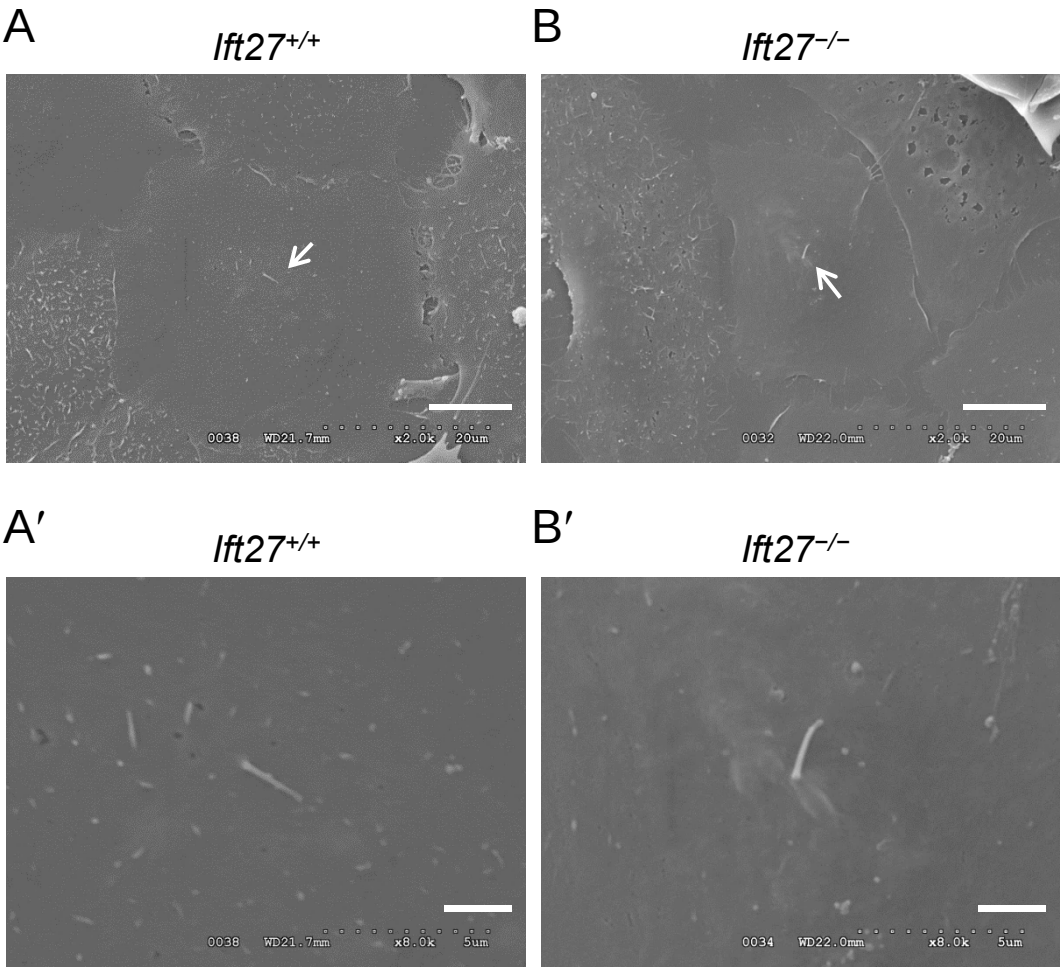

Fig. S8. Primary cilia in control (*Ift27*$^{+/+}$) and *Ift27* mutant (*Ift27*$^{-/-}$) the primary keratinocytes by scanning electron microscopy. (**A**) Cilium in a control cell. (**B**) Cilium in a mutant cell. A′ and B′ are enlarged areas of cilia shown in A and B. Scale bar: 10 µm in A and B; 2 µm in A′ and B′.

Fig S9

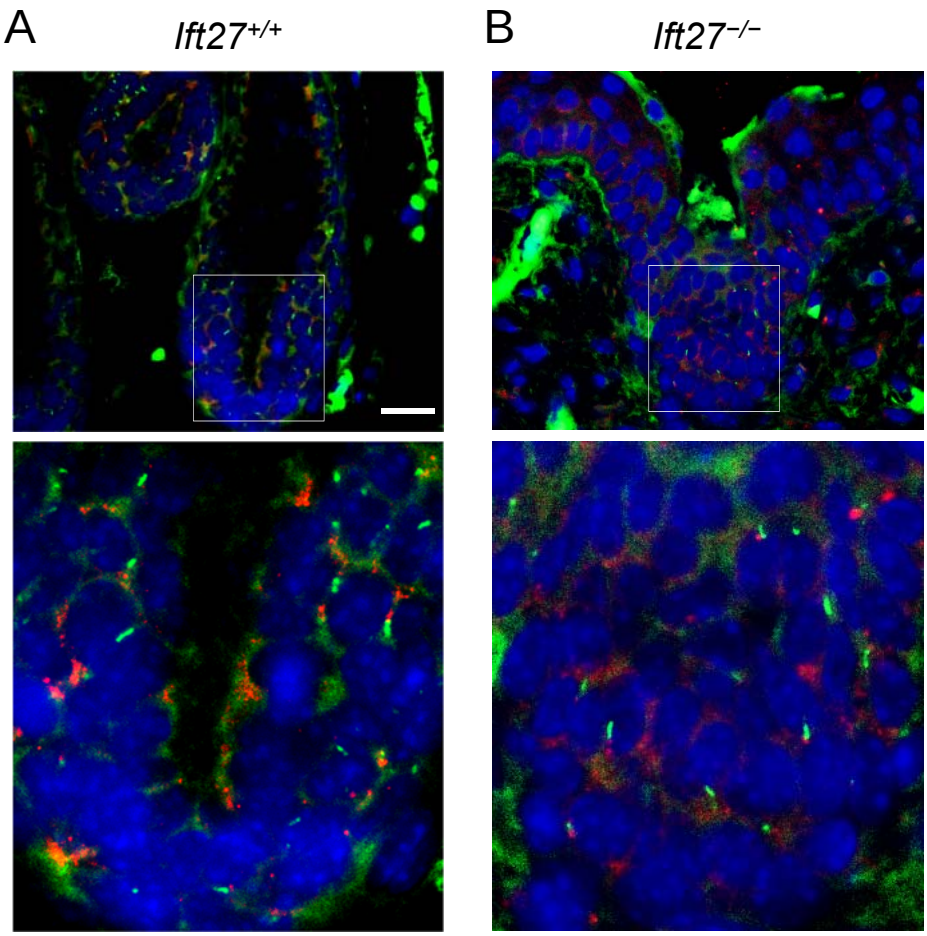

Fig. S9. Primary cilia in control (*Ift27*$^{+/+}$) and *Ift27* mutant (*Ift27*$^{-/-}$) skin transplants. (**A**) Cilia (ARL13B, green) and basal body (γ-tubulin, red) in hair follicles of *Ift27*$^{+/+}$ skin transplants. (**B**) Cilia (ARL13B, green) and basal body (γ -tubulin, red) in the hair follicle-like invagination of *Ift27*$^{-/-}$ skin transplants. Lower panels are enlarged boxed areas above. Scale bar: 20 μm.